AN ABSTRACT OF THE THESIS OF

SHUFA F. DWAN for the degree of MASTER OF SCIENCE

in GEOPHYSICS presented on JAN. 10, 1986

Title: A SEISMIC REFRACTION STUDY OF THE MONTEREY DEEP SEA FAN AND A COMPARISON OF VELOCITY STRUCTURES AMONG FAN SUBUNITS

Redacted for Privacy

Abstract approved: _____

R. S. Jacobson

A deep source-receiver seismic refraction experiment was conducted on the upper part of the Monterey Deep Sea Fan. The aim of this thesis is to construct the velocity structure of the upper Monterey Fan and to examine the lateral seismic velocity variations among the upper, middle and lower fan subunits. Using primary waves and whispering gallery phases (the multiply-reflected refraction waves), the sediment velocity structure was modeled by the tau-zeta travel time inversion process. The changes in velocity gradients with depth of the upper Monterey Fan are morphologically similar to that found on both the Central Bengal Fan and the Nicobar Fan, an abandoned lower fan of the Bengal Fan Complex. The velocity gradient of the upper Monterey Fan at depth, 0.59 s^{-1}, is significantly lower than both the middle Bengal Fan (0.68 s^{-1}) and the Nicobar Fan (0.81 s^{-1}). The upper fan subunit, which is closer to its sediment source, is characterized by higher porosities caused primarily by a higher sedimentation rate than the lower fan subunits. Since seismic velocity is inversely related to porosity, the upper fan subunit should have lower velocity gradients and seismic velocities than the other fan subunits. If porosity and velocity variations exist, then these variations can be used to constrain various models of deep sea fan formation. No definite conclusion

can be drawn at this time due to a fault within 1 km of the Nicobar Fan site; however, a systematic velocity variation pattern of deep sea fans is revealed.

Some portions of the Monterey Fan data contain refracted waves which have bottomed within the underlying acoustic basement structure. The entire velocity structure was solved by both the general and the "stripping" solving schemes. The results of basement structure show a velocity ranging from 3.4 to 5.8 km/s indicating that the uppermost part may be pre-existing continental rise sediments.

A Seismic Refraction Study of the Monterey Deep Sea Fan and a Comparison of Velocity Structures among Fan Subunits

by
Shufa F. Dwan

A THESIS
submitted to
Oregon State University

in partial fulfillment of
the requirements of the
degree of
Master of Science

Completed January 10,1986
Commencement June 1986

Approved:

Redacted for Privacy

Assistant Professor of Geophysics
in charge of major

Redacted for Privacy

Dean of College of Oceanography

Redacted for Privacy

Dean of Graduate School

Date thesis is presented January 10, 1986
Typed by Jeng Nin Chou for Shufa F. Dwan

ACKNOWLEDGEMENTS

My most sincere thanks go to Dr. Jacobson, my major professor, for his guidance. His help and patience are deeply appreciated.

I wish to also thank Dr. Menke for his valuable guidance, reviewing my thesis, and serving on my committee. Without the Macintosh, which was donated by Dr. Menke, this thesis could not have been done within a limited budget which I could afford.

Thanks go to Dr. Shor of SIO for allowing me to analyze this data set, obtained under his direction. The Naval Ocean Research and Development Activity, which funded this engineering test experiment in 1978, has given their verbal agreement to allow me to undertake this analysis.

Special thanks go to my fellow students in Geophysics. Bruce Dubendorff helped me to overcome the culture shock and introduced some good and bad American style to my life. Haraldur Audusson has given me many great times in academic discussion and playing the "unnamed" game, which we invented together. Marijke van Heeswijk, a lovely young lady, has been a good friend since she arrived. I want to suggest to them and to Tom DeVries that 1986 is a good year to graduate. Donna Moore, a truely lovely lady, gave me lots of encouragement and pleasure, especially in my first year. Everyone else in the geophysics has given me great memories and pleasures. Their friendship is very much appreciated.

My most heartful thanks go to my wife, Melissa C. Dwan. Without her support, encouragement, and prayer, this work won't be complete now; especially since we moved to Texas. I dedicate this work to her.

Last, but not the least, thanks are extended to my lovely parents, their support was essential to the completion of this thesis.

TABLE OF CONTENTS

LIST OF FIGURES

LIST OF TABLES

A SEISMIC REFRACTION STUDY OF THE MONTEREY DEEP SEA FAN AND A COMPARISON OF VELOCITY STRUCTURES AMONG FAN SUBUNITS

INTRODUCTION

Seismic velocities of marine sediments are controlled by complicated interactions of overburden pressure, temperature, lithification and sediment type. Deep sea fans are the ideal places to study the lateral variations of seismic velocity of marine sediments because of the thick sediment covering large areas. An 11 km long deep source, deep receiver seismic refraction experiment was conducted on the upper part of the Monterey Deep Sea Fan. A homogeneous constant velocity gradient layered model was inverted from the refracted wave travel time data by the modified tau-zeta inversion technique (Jacobson et al., 1984). The final result was compared with the velocity models of two similar experiments in the middle Bengal Fan (Dorman and Jacobson, 1981; Jacobson et al., 1981) and the Nicobar Fan, one of the lower fans of the Bengal Fan Complex (Jacobson et al., 1984). The objectives of this analysis are to examine the velocity structure of the upper part of the Monterey Deep Sea Fan and to test the hypothesis that different fan subunits have different and predictable seismic responses.

Geophysical studies of marine sediments have been improved due to various new techniques in both data collecting and processing during the last few decades. In a series of papers by Dorman (1979), Dorman and Jacobson (1981), Dorman (1983), Jacobson et al. (1984) and Bee and Jacobson (1984), a new experimental design and data analysis technique was developed. The tau-zeta inversion technique inverts the reparameterized travel time and range data into a number of layers with

constant velocity gradients. Using both the deep water acoustic sources and the digital recording seafloor hydrophones, a seismic record section with high resolution was obtained. The troublesome masking effect of the direct water waves, which generally arrive before the refraction waves, was removed by placing receivers on the sea floor. The subbottom structure was examined more precisely by the high frequency seismic waves and the high digital sampling rate in the record section.

The lateral and vertical variations of compressional wave velocity (hereafter called velocity) of deep sea fan sediments is dependent on several related factors, such as porosity reductions, density increases, degrees of lithification, overburden pressure increase, regional and vertical change in temperature, sizes of sediment grains and types of interstitial fluid. Of all factors, porosity appears to have the most influence on sediment velocity. Porosity reduction is mainly caused by the increase of overburden pressure. The relationship of burial depth and pressure makes velocity sensitive to porosity reductions with depth (Sheriff and Geldert, 1983). Hamilton (1979) examined the three important major factors of velocity gradients: pressure, temperature ,and lithification. The effects of these three factors were evaluated quantitively under some assumptions.

In this research, a velocity gradient profile from each of the three subunits of deep sea fan (the upper Monterey Fan, the middle Bengal Fan, and the Nicoban Fan), all using the same experiment design and analysis scheme, will be examined to evaluate the lateral variation of seismic velocity on deep sea fans. These profiles show remarkable similarities in the decreasing velocity gradients with depth, and the velocity gradients of each profile all reach asymptotic values within 1 km of depth. The comparison of the velocity gradient profiles reveals the lateral variations of velocity among fan subunits; consequently, the possible causes of the

lateral velocity variations are examined.

In the Monterey Fan data, strong coherent waves arrive slightly before the direct water waves and are identified as shallow refracted multiples. These multiples, the whispering gallery phases, propagate through the high velocity gradient layers in the upper sediment structure and reflect one or more times at the seafloor interface. The uppermost sedimentary layers, where the velocity gradient change the most rapidly, usually are not detected by shot-receiver surface geometries. The whispering gallery phases offer valuable information about the uppermost sediments.

Detailed measurements of velocity gradients in the Central Bengal Fan (Dorman and Jacobson,1981) and the Nicobar Fan (Jacobson et al.,1984) showed lateral velocity variations. A preliminary examination of lateral velocity variation from only two stations revealed both the similar morphological changes in vertical and systematic lateral changes in velocity gradients. A upper fan station was needed to complete this investigation. Since no similar seismic experiment had been conducted on the upper Bengal Fan, the upper Monterey Fan data is used to augment the data to examine the lateral velocity variation within deep sea fans. Sedimentation rate was concluded as the major factor determining the changes of lateral porosity, which is the most important factor in determining the seismic velocity (Jacobson et al.,1984). Within a same fan subunit, the difference in sediment lithology is not significant, except possibly within the main fan-valley. The comparison of the three velocity gradient profiles from two different fan systems to examine the possible cause is unbiased since most of the major factors which influence velocity are general in nature and not regional. Surface velocity gradients in different parts of the Bengal Fan Complex were reported by Hamilton et al.(1977) and Bachman et al.(1983). Similar surface velocity gradients in the Central Bengal Fan, 1.87 s^{-1} from

Dorman and Jacobson(1981) and 1.94s^{-1} from Bachman et al.(1983), were noted. In the Nicobar Fan, significantly different surface velocity gradients, 2.23 s^{-1} from (Jacobson et al.,1984) versus 1.62 s^{-1} from Bachman et al.(1983), were also noted and will be discussed in the following chapter.

DEEP SEA FAN GEOLOGY

Deep sea fans, developing at the base of a continental slope, are predominantly terrigenous deposits and are formed as fan-shaped bodies by long-term turbidite activities. Either a beach-canyon or a river-delta can act as a conduit bringing sediments of continental materials to the sea floor. Canyons generally cut backward through the base of continental slopes, sometimes even reaching continental shelves, and extend downward to the fan-valley system, which distributes sediments over an extensive area within the deep sea fan. The sediment distributary system is composed of one or more main fan-valleys and numerous small channels. Near the mouth of the submarine canyon, the turbidity current enter this distributary system. When the gradient of the sea floor decreases, the velocity of turbidites decreases; therefore, sedimentary grains within the turbidite flow begin to settle down on the floor due to the force of gravity. Below the mouth of a canyon, terrigenous sediments build up a broad, half-cone shaped depositional feature. These features were named "Deep Sea Fans" by Menard (1955). Off large river deltas, similar features are built and were called "Abyssal Cones" by Ewing et al.(1958). These features, composed of clastic sediments, have the same shape; therefore, they will be called fans (deep sea fans) hereafter.

Normark's Model

A general growth-pattern model of deep sea fans was proposed by Normark (1970a, 1978) by studing the simiarities in morphology, structure and surficial-sedimentation patterns among modern deep sea fans. In Normark's model, deep sea fans principally have three distinct morphologic

divisions, called the upper, middle, and lower fan sununits, which are related to different facies associated with sandy and coarse turbidites (Fig. 1). The upper fan has large-leveed valley(s) in which the coarsest sediments of the fan are deposited. Sand content of the sediment of the levee decreases with increasing distance from the axis of the fan-valley (thalweg) because overflow over the bank is the major sediment source for levee sediments. The middle fan or suprafan is recognized as a convex-upward depositional lobe with active sand deposition at the terminus of the leveed fan valley. The coarsening and thickening upward sequences of sandy turbidites on the upper suprafan are cut by numerous channels, channel remnants, and isolated depressions. The lower suprafan is generally free of those channel features and has a reasonably smooth topography. The lower fan area is characteristically free of coarse grained turbidites and channel features. Sediments on the lower fan are nearly flat-lying or ponded; therefore, this region is morphologically indistinguishable with basin-plains or abyssal-plains in many areas. Local basin shapes, and the type and the rate of sediments supplies determine the relative proportions of each fan subunit.

The fluctuation of sea level related to the Pleistocene glacial cycle has had a strong influence on the sediment supply of deep sea fans; moreover, the rapid sea-level rise in the Holocene has left many modern fans without a source of coarse clastic sediments. Therefore, the original morphologic features are either preserved with a thin mud blanket above or eroded by bottom currents. On the Monterey and the La Jolla Fans, erosion within the main valley system has resulted in sediment bypassing the upper and middle fan regions; therefore, occassional overbank muds are the only turbidite deposition on the upper and middle fan in this area (Normark, 1978). The San Lucas and the Navy fans have received little or no turbidite

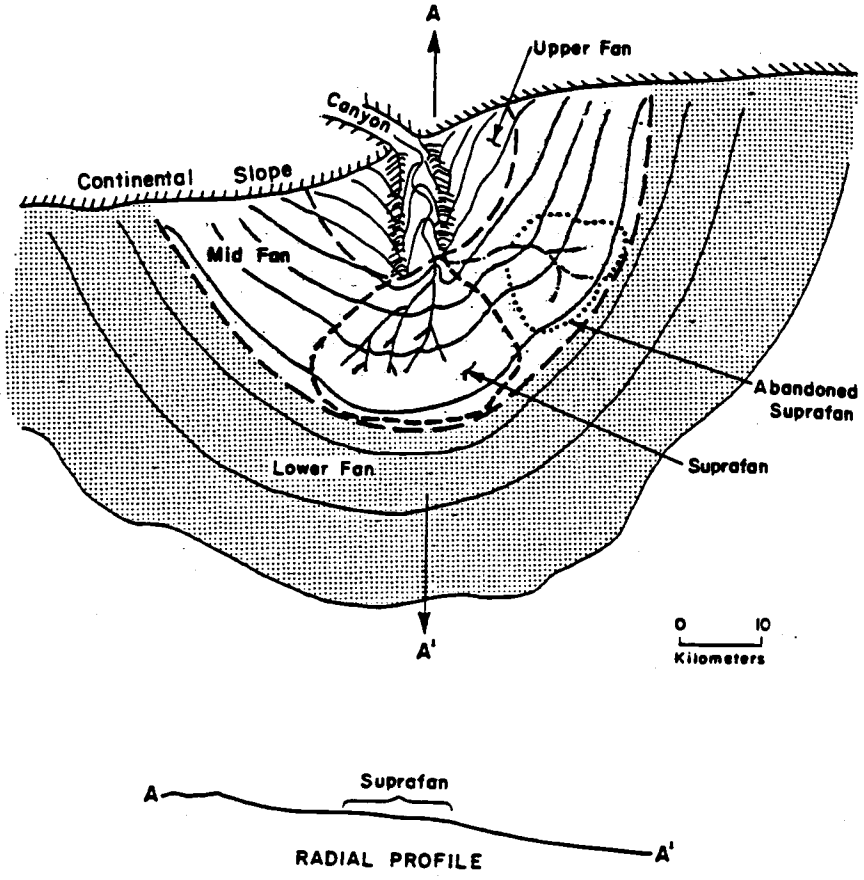

Figure 1. Schematic representation of the model for submarine fan growth emphasizing the suprafan area (From W.R., Normark, 1978).

sediments during this period; their original morphologic features are unaltered and are only blanketed by a thin Holocene hemipelagic mud. Slight modification of the Astoria and Amazon fans have been found, but the original morphologic features are recognizable. Therefore, the principal geological features on deep sea fans are still the same as in its growth stage.

The Bengal Fan, the world's largest deep sea fan, does not exhibit the suprafan feature, which is the most characteristic feature in Normark's fan model. Normark (1978) argued that the restricted grain-size distribution and the supply rate of the sediment influx can determine whether a suprafan structure can form. Most likely, the distinctive suprafan feature will develop in a canyon-fed deep sea fan. In the upper Bengal Fan, an extensive system of large leveed fan-valleys reveals little internal structure from seismic profiles and cored samples on the levees. These results imply a rather uniform grain size within sedimentary deposits. Instead of depositing below the valley terminus, those fine grain sediments may spread laterally as overbank deposition near the valley terminus due to the energy loss of turbitide flows. The suprafan feature may not have occurred or has only resulted in small scale. Therefore, the distribution of sediment supply may be the key factor affecting the morphology of deep sea fans (Normark,1978).

Mutti and Ricci Lucchi's Model

Mutti and Ricci Lucchi (1972) published a deep sea fan model based on sedimentological characteristics of the ancient rock studies from the northern Appennines, Italy. Based on lithology, size, and the geometric

distribution of channel sequences, the entire fan area was divided into five distinct depositional zones: slope, inner fan, middle fan, outer fan, and basin plain. The main difference between Normark's model and Mutti and Ricci Lucchi's studies is the scale of those geological features. Normark's morphologic subunits are based on features on the scale of tens of kilometers, but Mutti and Ricci Lucchi's depositional subunits are characterized by features a few kilometers at most. Shanmugam and Moiola (1985) pointed out that the terminology of the two models is nearly identical except that the proposed boundary between channelized and non-channelized sequences occurs in the middle fan, or suprafan, of modern fans and in the outer fan of ancient fans.

Based on a study of the deposition of the Hecho group, Spain, a modified model with detached lobes and a bypassing zone (Fig. 2) was proposed (Mutti and Ricci Lucchi,1975). These differences reflect fundamental changes in fan behavior and lobe development, allowing the use of these new features to be incorporated into as a predictive model. Bachman et al.(1983) used the bypassing model to explain the lower near-surface velocity gradients of the lower Bengal Fan compared with the gradients of the Central Bengal Fan. Mutti (1979) claimed that a hydrodynamic readjustment of turbidity flows in front of channel mouth results in a nondeposition and a related zone of bypassing. Walker (1980) argued that the form of a bypassing zone seems unlikely because the tendency of turbidity flow to spread and sediment grains to deposit before reaching the channel terminus. Furthermore, the reduction of current velocity from channelized turbidity flow to unchannelized spreading flow seems more likely to result in deposition rather than a bypassing zone. A hydraulic jump effect was illustrated by Shanmugam and Moiola (1985, Fig.3) to form a possible bypassing zone. This special condition requires a

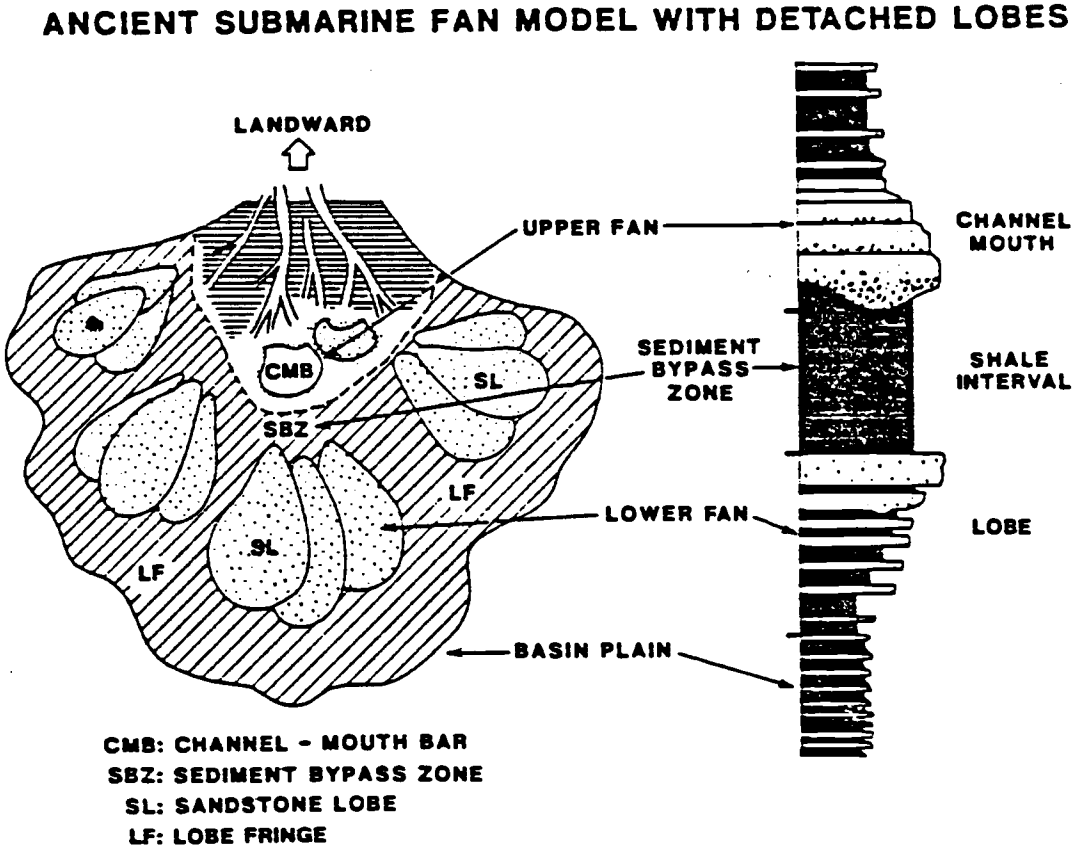

Figure 2. Schematic representation of the model for ancient submarine fan with detached lobes (From Mutti and Ricci Lucchi, 1975).

sudden increase of slope, and the Boltana Anticline in the Hecho Basin in Spain, can provide this type of tectonic influence. Basically the increase in slope and a related reduction in flow height will increase the flow energy and can result in a bypassing zone along the other side of the slope. However, the tectonic control of bypassing can not be generally applied as a basic fan model. Therefore, more field data from both modern and ancient fans and more hydrologic experiments are needed to examine the bypassing model.

Turbidites

The typical turbidite consists of sand layers with interbedded finer grained pelagic sediments. Due to the episodic activity of turbidity currents, the mix-layered structure always can be found in a fan structure. Four main facies of turbidites can be classified by the different sedimentary environments (Blatt et al., 1972). They are: 1) Channel deposits composed of sands and pebbles, which are caused from grain flow deposits. 2) Proximal turbidites relatively close to the sediment source. These structures are marked by massive, poorly developed tractional structures, relatively weak grading, and little interbedded pelagic clay and terrigenous mud. 3) Turbidites of the classic type with distinct graded bedding, interbedded pelagic clays, and oriented erosion. It also has the fill marking at the base of the sand layer known as sole marks. The famous Bouma sequence (Bouma, 1962), known as the successive sedimentation structure, can be found in this enviroment. 4) Distal turbidites, the furthest deposits from the sediment source with thin, fine-grain interbedded turbidite layers.

The Bouma sequence is marked by rapid deposition, modeled by five layers making a complete sequence of turbidites. The first four layers are

deposited from turbidity currents and decrease in grain size upward from massive, graded sand to sand-silt with parallel laminar structures; the uppermost layer consist of very fine sediments. The complete Bouma sequence is seldom found; most studies generally show a lack of one or two layers.

Walker (1978) presented a good review of the ancient submarine fan deposition model, relating facies, fan morphology, and depositional environment,within the framework of the morphologic subunits of modern fans (Fig. 3). The levees of the upper fan are composed of fine grained alterations of thin sandstone and mudstone layers. The upper part of the suprafan region shows massive and pebbly sandstone deposits with lenticular bedding. When the channels on the upper part of suprafan change position, the sand bodies tend to coalesce and will scour any fine grain deposits between the channels. The classic Bouma sequence can be found in this area. The lower fan is characterized by hemipelagic deposits with interbedded turbidites. In the stratigraphy of a prograded fan, a major coarsening upward sequence can be found; nevertheless, the fining upward sequences still dominate in the upper parts of deep sea fans (Walker, 1978, Fig. 14).

In 1982, an international deep sea fan meeting was hosted by Gulf Research and Development Company (COMFAN, 1984). The main aim of the meeting was to analyze previous results and discuss the different concepts between the studies of modern and ancient fans. The discussion emphasized the major influences upon deep sea fan formation, such as tectonic setting and sea level variations, amounts and types of sediments supply, sedimentation rates, different natures of fan growth, facies distribution, and stratigraphic sequences. Deep sea fans were divided into three categories: enlongate fans, radial fans, and slope aprons (Stow et

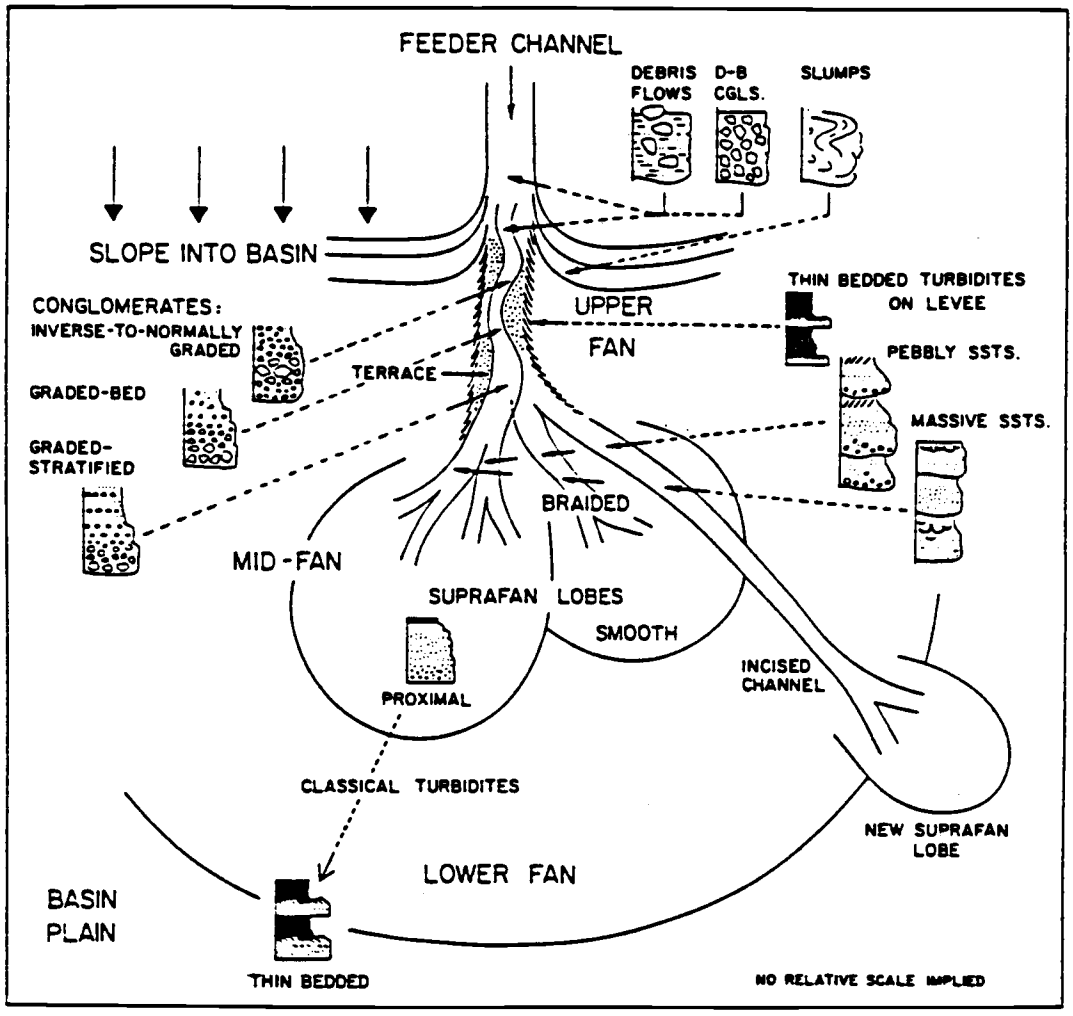

Figure 3. Schematic model of submarine fan deposition, relating facies, fan morphology and depositional enviroment (From R.G., Walker, 1978).

al.,1984). With medium to high sediment input of mostly mud and fine sand, elongate fans usually develop. Elongate fans have characteristics similar to the highly effective fan system of Mutti and Ricci Lucchi and the delta-fed fan system of Normark. Radial fans, similar to the poorly effective fan system and the canyon-fed fan system, result from reduced sediment input with a higher sand/clay ratio. Slope aprons are not true fans, but are closely related turbidite systems. Stow et al. concluded that the Bengal Fan is a typical elongate fan and the Monterey Fan lies between the radial and the elongate types. However, no detailed explanation was provided about how this classification was determined.

A distinct morphological apex on the axis of any deep sea fans always can be found because of the fixed position of the sediment source. The sediment distributary system consist of one active leveed fan-valley on the upper fan, numerous ephemeral small channels on the middle fan, and sheet-like flow on the lower fan with no channel. Depositiions from the turbidity currents are generally localized in time and space. To have broad, uniform depositional structures on deep sea fans, the fan-valleys apparently need long periods of rapid changes in position to cause the random depositions of sediments. Both channel piracies of the Monterey Fan (Normark, 1970b) and the Bengal Fan (Emmel and Curray, 1981) reveal the complicated growth history of deep sea fans. Asymmetrical outlines sometimes are observed in deep sea fan profiles. Normark (1978) argued that those older and/or more rapidly growing fans will display a symmetrical outline except when they are still in the youthful developing stage. Most of the deep sea fans do not correspond with Normark's deep sea fan model in every aspect, but the general morphology is followed. The various regional effects such as tectonic activity, basement topography, and the restricted grain sizes of the sediment influx source can change the growth patterns of

the fan, resulting in various morphologies. Normark's general fan model is based on the study of the surface morphology and sedimentation patterns of modern fans. The physical properties of deeply buried sediment, such as the porosity -depth profile, can be derived from the velocity-depth function in seismic refraction studies. Elevated porosity implies a location of rapid sedimentation, which is the main difference between suprafans and the by-passing zone hypotheses. An elevated porosity structure will result in an area of rapid sedimentation due to the continuously depositing sediment with a high internal water content. Furthermore, only the deep sediment structure might provide the information concerning the original fan growth if no severe erosion has been happened. Therefore, geophysical investigations can help to achieve a better understanding of the deep sediment structure, enabling correlation of the physical properties with different fan subunits, a still uncompleted area in deep sea fan research.

THE MONTEREY DEEP SEA FAN

Fan Setting

The Monterey Deep Fan, covering 100,000 km^2 in area, is the largest modern marine fan off the California coast. The fan lies between Monterey Bay and Pt. Arguello in the central California (Fig. 4). The Monterey Fan is named after the largest and deepest of its three major submarine canyon groups, Monterey, Ascension, and Lucia-Partington (Shepard and Dill, 1966). The Monterey Fan-Valley, continuous with the Monterey Canyon, extends about 300 km south-southwest across most the fan. Two other inactive fan-valleys, the Ascension and the Monterey East Fan-Valleys, join the Monterey Fan-Valley on the surface of the upper fan area. The turbidite nature of the Monterey Fan has been fully supported by the provenance of the the sand-size particles, the depositional fabric and sedimentary structure, the location of coarse deposits in the axis of channels and the levees structure on the upper fan (Dill et al., 1954; Menard, 1960; Wilde, 1965; Shepard, 1966; and Wilde et al., 1978).

The Monterey Fan is built on oceanic crust of Oligocene age from 23.7 to 36.6 m.y. (based on the magnetic anomaly time scale) which formed along the Pacific-Farallon spreading center, which subducted under central California about the late Oligocene (Atwater, 1970). Due to movement along the San Andreas Fault system, the fan has been moving northwest relative to the North American plate in Neogene, but the slope segment of the canyons probably have moved with the fan, based on the persistent sediment pathways during fan growth. The fan probably did not begin to develop until the Latest Oligocene or Early Miocene when turbidity currents from California margin could reach the fan area (Normark et al., 1984).

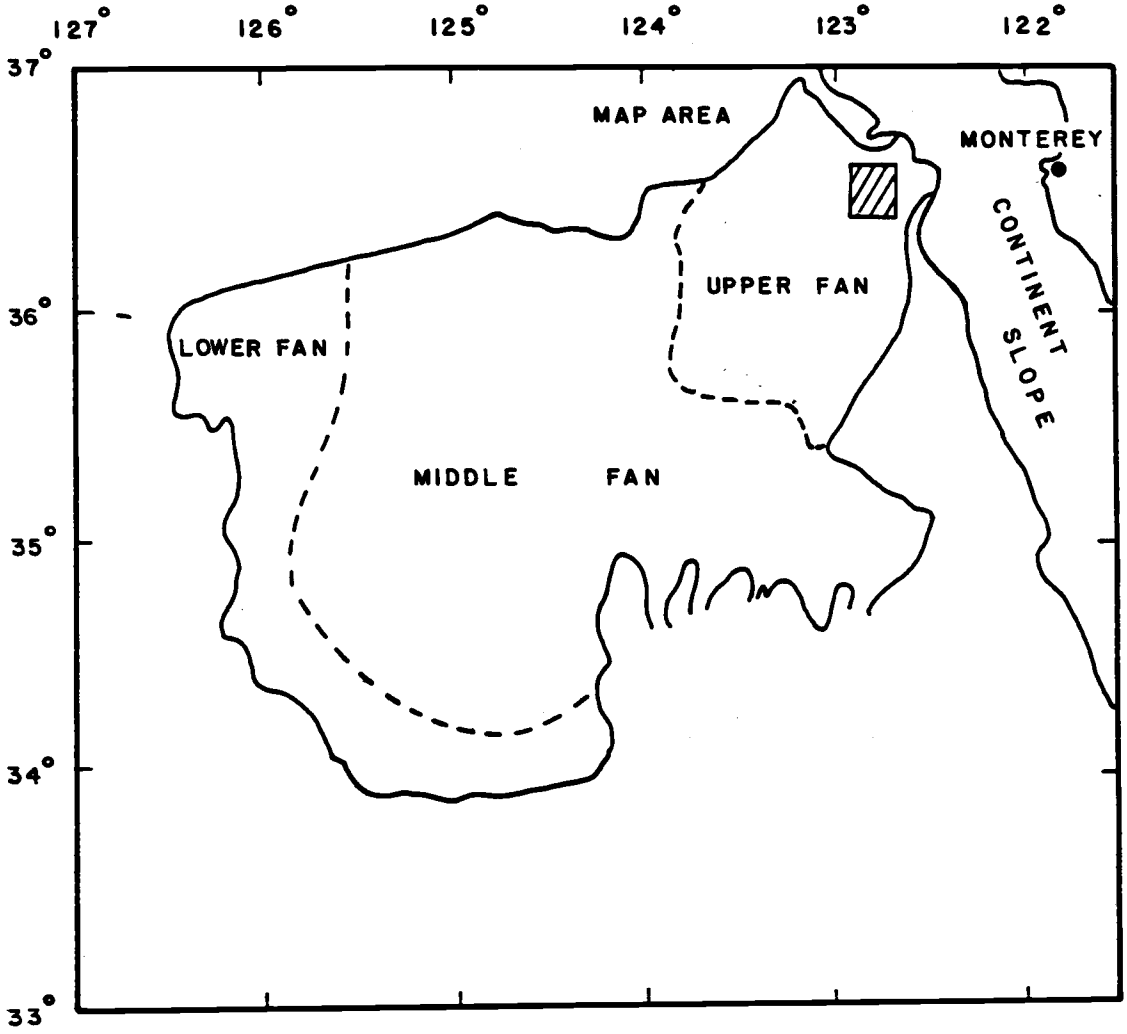

Figure 4. Schematic map of the Monterey Deep Sea Fan showing fan subunits and the location of refraction site (shadowed) (modified from Normark et al., 1983). The deep sea fan is divided into three subunits: the upperfan, the middle (or superafan), and the lower fan.

The Monterey Canyon system have been studied by numerous scientists in the past, but the Monterey Fan did not attract much attention. Dill et al. (1954) first described the fan. Menard (1960) discussed the origin and age of the fan, and Wilde (1965) studied the extent and physiography of the fan from bathymetric and surface sediment data. Moreover, Shepard (1966) showed the Monterey fan-valley does continue with the Monterey Canyon forming a "horseshoe" shape meander on the lower part of the upper fan. Normark (1970b) used seismic reflection profiles across the fan to evaluate the relationship between the fan-valley system and the overall growth of the fan. Since the last few years, more geloogical research on the Monterey Deep Sea Fan has been published, e.g. Chase et al. (1975), Hess and Normark (1976), Wilde et al. (1978), and Normark et al. (1980, 1984).

Upper Fan

According to Normark's morphologic subunits, the entire Monterey Fan can be divided into three different morphologic divisions: the upper fan, the middle fan, and the lower fan (Fig. 4). The Monterey Fan-Valley is the most prominent feature on the entire fan; the fan-valley acts as the main conduit to transport the turbidity current to the deep sea floor. Some fundamental changes of the fan-valley have been noted, such as the channel piracy and the change from the depositional nature to the erosional nature. The fluctuation of sea level related to the Pleistocene glacial cycle, has had a marked effect on the Monterey Fan. Due to the sea-level rises, the sediment supply was reduced sharply in content and has shifted to a finer grained sediment. Normark et al. (1984) argued this effect would not be prominent at the beginning of the Monterey Fan development because

both the Ascension and the Monterey Fan-Valleys back-cut to the outer continental shelf and across the shelf respectively. After changing the nature of the fan-valley from depositional to erosion, the Monterey Fan-Valley now is extending downward carrying most of the sediment beyond the upper fan and the middle fan. The mechanisms for initiating the channel piracy and the changes of fan-valley nature are not well understood at this time. However, the world wide sea-level rise must play an important role in both cases.

Depositional fan-valleys are always bounded by natural levees built up by the over-flow deposits from the main fan-valley. With depositional fan-valleys, coarse sands are deposited on the valley floor, while fine sands, silts, and muds are deposited on the levees. The sand content on the levees decrease with distance from the fan-valley axis. During aggradational stages of depositional fan-valley, thick and coarse sands grading to gravels are characteristic of the depositional development. Normark (1978) pointed out that the coarse-grained channel-fill sequences are the basic sedimentary facies for the upper fan. Before the channel piracy (Normark, 1970b), the old Monterey and the Ascension Fan-Valleys were two independent, depositional fan-valleys. Due to the tilting of the surface of the channelized turbidity current flow, both fan-valleys have large western levees, which are the right side of channel (looking downstream) (Menard, 1955). The Ascension Fan-Valley did not develop a mature eastern levee because of the encroachment of the well-developed western levee of the old Monterey Fan-Valley. Because the different sedimentary deposition rates of each fan-valley, the floor of the old Monterey Fan-Valley was higher than the Ascension Fan-Valley, so a break along the western levee of the old Monterey Fan-Valley may have started the piracy. After the breach, the old Monterey Fan-Valley captured the lower part of the

Ascension Fan-Valley and abandoned its original lower part valley, now called the Monterey East Fan-Valley.

Erosional fan-valleys can be caused by either changes in rates or types of sediment influx or a tectonic setting. The turbidity currents cut into the previous sediments to form the erosional channel, resulting in sediment bypassing most of the fan area. Normark et al. (1984) stated that the Monterey Fan-Valley piracy happened slightly before or about the time when the east pass of sediment flow in the Chumash Fracture Zone was formed, but the relation between the formation of the east pass and the piracy was not described.

In the upper fan, the Monterey and the Ascension Fan-Valleys and the complicated leveed structures, are the main morphologic features (Fig. 5). The dominate lithology of the large levees is sand and silty mud (Normark et al. 1984). Hess and Normark (1976) stated that coarser grained sands were found in the valleys and channels, and fine grained sands and silt muds were found on the levees on the upper fan. The internal structures of levees are basically lens-like with convex upper surfaces. A single channel analog recording seismic reflection profile (Fig. 6) shows a clear, layered horizontal sediment structure and the lens-like, convex upward face along the western levee wall. Normark (1970b) stated that the western bank of the Monterey Fan-Valley has the best developed levee structure. The reflection profile shows a highly stratified, homogeneous-looking layered structure. A highly reflective body below the crest of western levee wall in the reflection profile (Fig. 6) extends upward and eastward to the current fan-valley floor. From its high reflectivity which is the same as the coarse sand on the valley floor sand, the body is interpreted as the deposit of coarse grained sand on the old valley floor. Therefore, the fan-valley must have been migrating eastward.

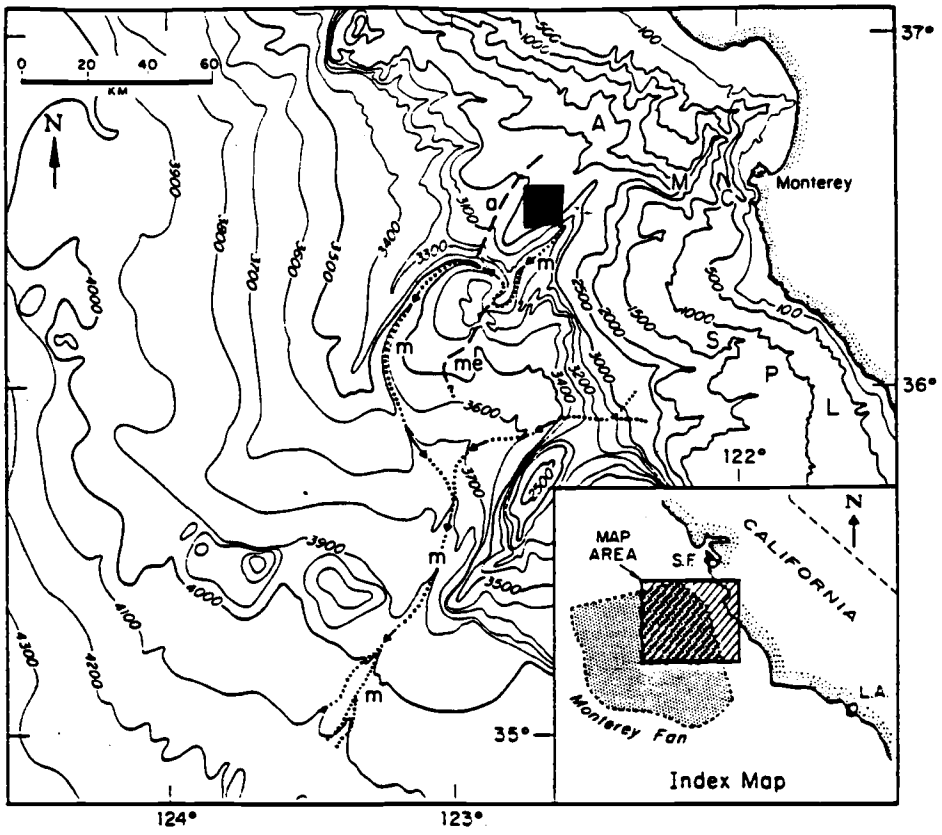

Bathymetry of the study area on the Monterey Fan (after WILDE, 1966) with the contour interval in meters. San Francisco and Los Angeles are shown on the index map. Capital letters denote submarine canyons; these are, from north to south: A = Ascension, M = Monterey, C = Carmel, S = Sur, P = Partington, L = Lucia. Lower case letters denote fan-valleys: a = Ascension, m = Monterey, me = Monterey East. The axis of Monterey Fan-Valley is indicated by the dotted line; the two short dashed line segments denote the axes of Ascension and Monterey East Fan-Valleys. The horseshoe meander of the Monterey Fan-Valley is at 36° 15'N and 122° 50'W.

Figure 5. Bathymatric map of the Monterey Deep Sea Fan, showing the location of the refraction site (shadowed) between the Monterey (m) and Ascencion (a) Fan Valleys (From W.R. Normark, 1970b). The "horseshoe" meader is south of the shadowed area.

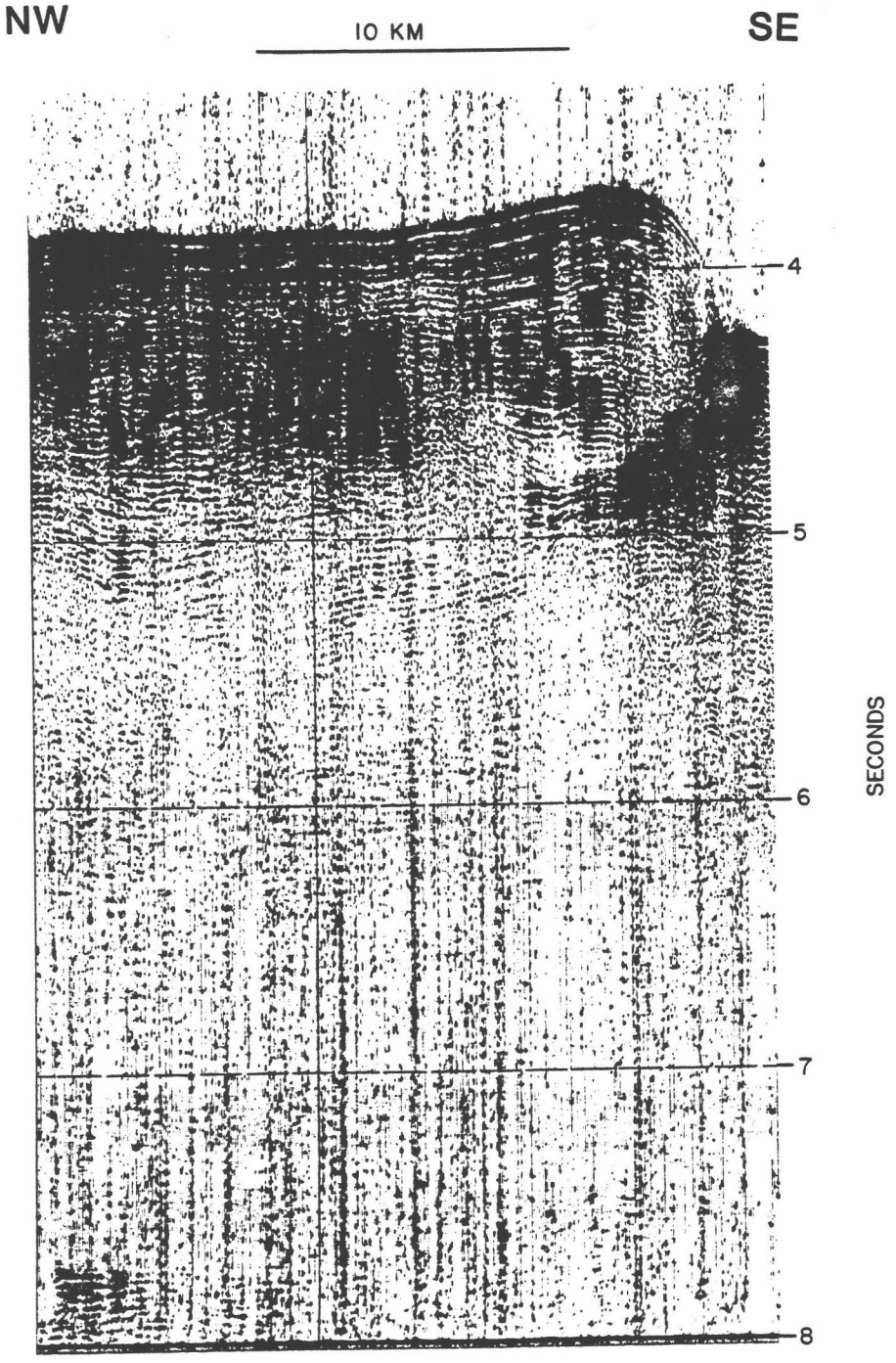

Figure 6. Single channel seismic reflection profile across the NW levee of the Monterey Fan Valley. The seismic refraction line was run along the same line of reflection section, NW of the highly reflective body underneath the levee.

This interpretation is in accord with Menard's (1955) prediction that the channel often achieves its present position through migration away (eastward) from the always higher west levee wall.

Middle and Lower Fans

In the middle fan, no obvious suprafan structure have been found. The depositional conditions of three distinct parts in the middle fan were examined by Normark et al. (1984). A depositional feature below the active Monterey Fan-valley was noted as the potential area for developing a suprafan. The southern middle fan is currently fed directly by the main Monterey Fan-Valley. Most sediment is carried through the area by the continuous leveed channel from the main fan-valley. The turbidity current emptied at the south end of this area, where a smooth base level has not yet been established. This area show a strong, diffuse reflection on seismic profiles, impling a sand-rich environment. The western middle fan has received the sediment from overflows of turbidity current from the main Monterey Fan-Valley. Reflection profiles show that this area may be the least sandy of the middle fan area. Very few channels and valley features have been found in the western middle fan. The southwest middle fan is an abandoned depositional lobe since only small amounts of sediment has passed through the western pass of the Chumash Fracture zone. The lower fan presents a channel-free, flat-lying morphology. The lower fan area receives the over-bank turbidite flow as its major source which is similar as the western middle fan. Normark et al. (1984) pointed out that a ponded structure may be formed due to a distinct break in the slope

gradient over several kilometers.

Hess (1974) measured 5 core samples in different parts of the Monterey Fan for Holocene sedimentation rates. The results show a systematic decrease with increasing distance from the sediment source (Wilde et al.,1978,Table 1B). The sedimentation rates of Holocene sediment were estimated about 432 m/m.y. (19P) in the upper fan and decrease to 32 m/m.y. (187G) in the lower fan. This systematic variation of Holocene sedimentation rates implies that the by-passing model is unlikely in the Monterey Deep Sea Fan at least in this period.

PREVIOUS GEOPHYSICAL STUDIES

Although marine seismic refraction studies have been conducted over the past forty years, the study of geophysical properties of deep sea fan sediments has not become successful until the last several years. Jacobson et al. (1984) mentioned three difficulties in the refraction studies of marine sediments in those early years: (1) the low density of data when explosive charges are used as sources, (2) the amount of water overlying the sediments acting to mask refracted arrivals from the upper sediment layer, (3) the conventional assumption of planer, isovelocity layers, which produces erroneous estimates of velocities and thicknesses. The first two problems can cause poor quality and less information within a record section, and the third problem will bias the velocity structure. Using airguns/waterguns and recording instruments at the seafloor, most of the problems caused by the first two can be solved; a clean record section can be obtained. The erroneous conception of the isovelocity layers in marine sediments was found incorrect by the evidences of positive velocity gradient in many studies (Hamilton, 1979; Houtz, 1980, Spudich and Orcutt, 1980, Dorman and Jacobson, 1981, and Jacobson et al.,1984). A layered model with constant velocity gradients is a more reasonable and accurate model in studying a thick marine sediment structure.

Deep Source-Receiver Refraction Studies

A newly designed seismic refraction experiment using seafloor hydrophones and deep acoustic sources was developed at the Marine Physical Laboratory, Scripps Institution of Oceanography,. This method had been first conducted on the Monterey Deep Sea Fan; afterward, it was used

on the Central Bengal and the Nicobar Fans in the Indian Ocean. Dorman and Jacobson (1981) and Jacobson et al. (1984) reported the seismic results from the Central Bengal Fan and the Nicobar Fan, respectively. Both profiles of velocity gradient versus depth show that the gradient decreases to asymptotic values within 1km of depth. The two profiles are morphologically similar but have significantly different asymptotic values, 0.67 s^{-1} for the Central Bengal Fan and 0.81 s^{-1} for the Nicoban Fan. The similarity in velocity structure indicates the systematic changes of the velocity structure in deep sea fans; moreover, the difference in the asymptotic values reveals the changes of depositional conditions among fan subunits. Jacobson et al. (1984) concluded that the vertical and lateral variations in velocity are controlled by the changes in porosity. The lateral variations in porosity can be explained by the difference in sedimentation rates over time among fan subunits and the local geologic condition of the Nicobar Fan.

Sedimentation rates over deep sea fans are related to the distance from the sediment influx source. A high porosity structure results from high sedimentation rate because the new sediments, which settle down on the sea floor with a high water content, will not reach the equilibrium condition of interstitial water due to the continuous deposition of sediments. Consequently, the results from the Nicobar Fan and the Central Bengal Fan imply a decrease of the sedimentation rates seaward. The low velocity gradients, which imply a high sedimentation rate in the middle fan subunit, favor Normark's fan model (Normark, 1970a, 1978), which suggests a higher sedimentation rate on the middle fan than on the lower fan.

Sonobuoy Studies

Seismic velocities do vary with position over deep sea fans. Hamilton et al. (1974,1977) and Bachman et al. (1983) determined velocities and velocity gradients as a function of subbottom travel time from several wide-angle reflection records on the Bengal Fan Complex. Near-surface minimum velocity gradients have been found in areas close to the sediment source where sedimentation rates are high, such as the upper part of the Bengal Fan. Similar cases also have been found in the Gulf of Mexico, the Amazon Cone and other places (Houtz, 1974, 1977, 1978, 1980, 1981). Using sonobuoy techniques, the near-surface velocity gradients were reported by Bachman et al. (1983) for the Nicobar Fan (1.62 s^{-1}), the Upper Bengal Fan (0.86 s^{-1}), the Central Bengal Fan (1.94 s^{-1}), and the Southern Bengal Fan (1.18 s^{-1}).

The surface velocity gradient in the Nicobar Fan (1.62 s^{-1}), as reported by Bachman et al.(1983), is different from the value (2..32 s^{-1}) reported by Jacobson et al.(1984). This value (1.62 s^{-1}) may characterize the Nicobar Fan as the major depositional area according to Mutti and Ricci-Lucchi's deep sea fan model. Jacobson (1984, written statement) pointed out that the moderate seafloor velocity gradient from the Nicobar Fan, which has has no deposition of turbidites in the last 5 million years, may be indicative of the effects of quiescent sedimentation and the consequent reduction in porosity at the sea floor. The deep velocity structure, which may not have had sufficient time to equilibrate with the cessation of high rates of sedimentation is a better index of its geophysical characteristics. Because of this, it is better to use the deep velocity structure rather than the velocity gradient near the sea floor in examing the physical properties of fan subunits.

DATA COLLECTING AND PROCESSING

In September 1978, a seismic refraction experiment was conducted as an engineering test of a new sea floor hydrophones system, which was developed at the Marine Physical Laboratory, Scripps Institution of Oceanography. The purpose of this experiment was to test the capabilities of the recording instruments and shooting procedures, which would be used for the later Bengal Fan experiment. The seismic refraction experiment was located in the area between the Monterey and Ascention Fan Valleys of the upper Monterey Fan (Fig. 4).

In this experiment, three digitally recording seafloor hydrophones (SFHs) were used as receivers, and explosives, detonated by SUS charges, were chosen as acoustic sources. The response of SFH is broadband (0 to 100Hz) with an antialias filter set at 80 Hz (Fig. 7) with an 126dB of dynamic range. The recording system includes an event detector which can detect the high frequency direct water wave and a circular memory buffer which can store the continuously incoming signals. When the direct water wave is detected, conversion of the analog signals into a digital signal continues for a predetermined amout of time. The refracted wave, which contains the information of subbottom structures, usually arrives before the direct water wave. Using the water waves reflected off the seafloor and/or the sea surface, which always arrive after the direct water wave, the shot-receiver range, the shot depth, and the travel time of the direct water waves can be determined. Therefore, the total length of the recording must contain a certain amount of data before and after the trigger event to make sure all necessary data are included. The explosive sources, 256 pounds of TNT detonated by an MK94Mod0 SUS charge (Naval Ordinance System Commands, 1973), were set to explode at the

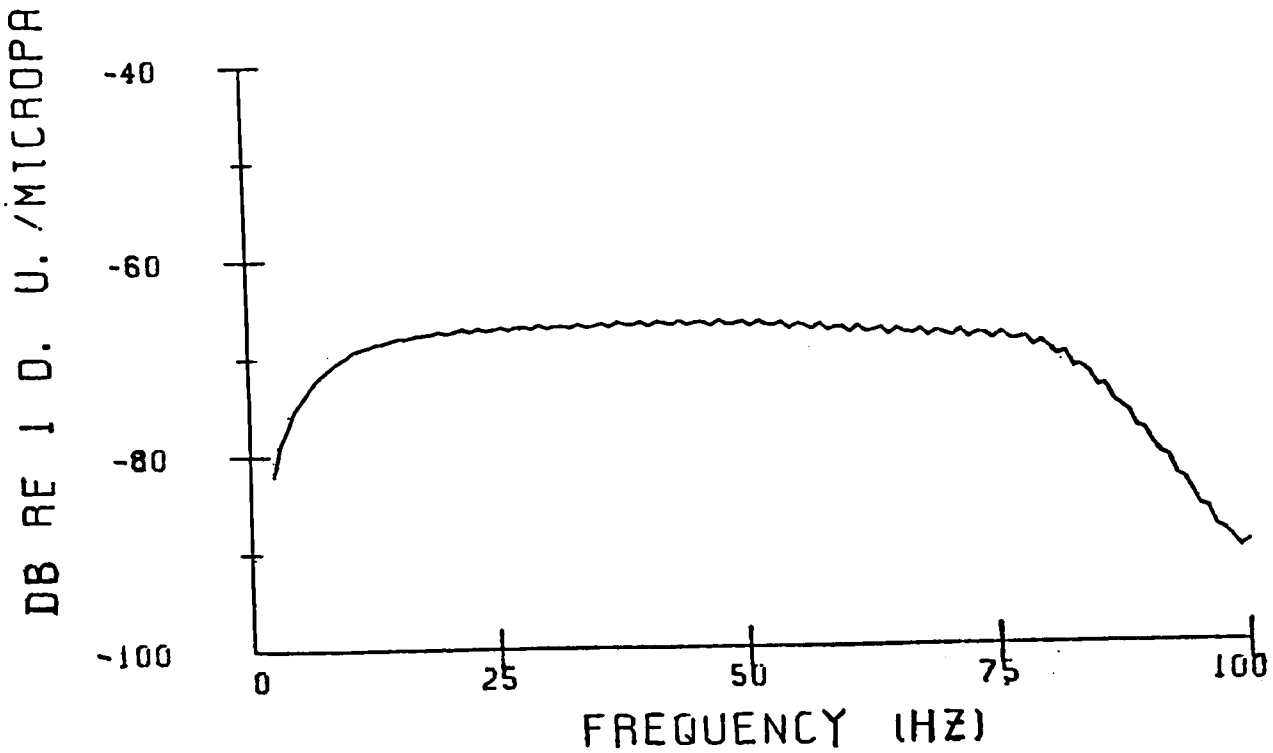

Figure 7. Instrument response, in dB re a digital unit per μ Pascal, as a function of frequency. The antialias, or low pass, filter has its corner frequency at 80 Hz. System response below 2 Hz is unknown hydrophone response at these frequencies.

hydrostatic pressure at the depth of 6000ft (1829 m). The experiment geometry was identical to those experiments described by Dorman and Jacobson (1981) in the Bengal Fan and Jacobson et al. (1984) in the Nicoban Fan.

A "T" shape shot line (Fig. 8) was conducted, and a total of 17 usable seismograms, containing the refracted waves and all three water waves, were recorded with a maximum range of 12 km. A single channel analog recording seimic reflection profile (Fig. 6) along the seismic refraction profile shows a rather smooth and flat sea floor with an average depth about 2880 m. The reflection profile also suggests a highly stratified, homogeneous-layered model should be a suitable velocity model for this study area. The refraction profile was placed away from the massive sand body under the western levee of the Monterey Fan Valley to avoid any anomalous refraction/reflection waves. The data from the upper Monterey Fan show much more complicated waveform patterns than either the Bengal Fan or the Nicobar Fan record sections. The major complication came from the refracted wave propagating within the underlying basement structure, having a higher velocity than the sediments. Most basement arrivals arrive before the sediment arrivals. The associated travel time triplication from the velocity jump between the sediment and the acoustic basement layer complicate the record section. Several branches of coherent secondary wave between the first arrivals (basement arrivals) and the direct water waves with relative large amplitudes were noted.

The first step in analyzing the seismic refraction data is to determine the shot depths, the shot-receiver ranges, and the travel time of the direct water waves. These parameters were determined by tracing rays through the water column (Fig. 9). A sample seismogram with refraction waves and

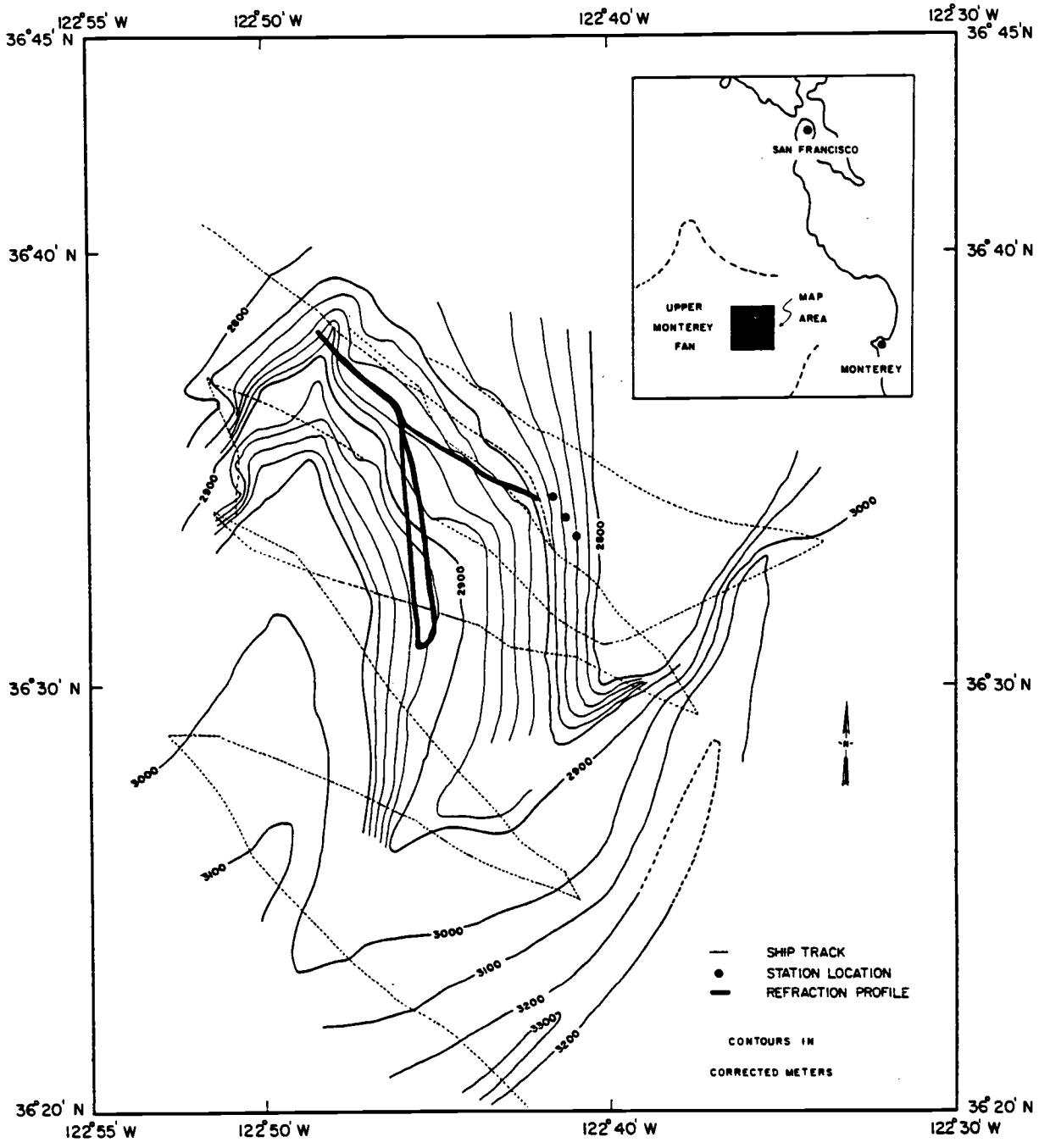

Figure 8. Detailed bathymetric map of the refraction site on the upperpart of Monterey Deep Sea Fan is shown with the refraction line and instruments locations. Based upon bathymetric profiles collected during the cruise and available low resolution bathymetric charts. Contours in conrrected meters. The numbers correspond to instrument numbers.

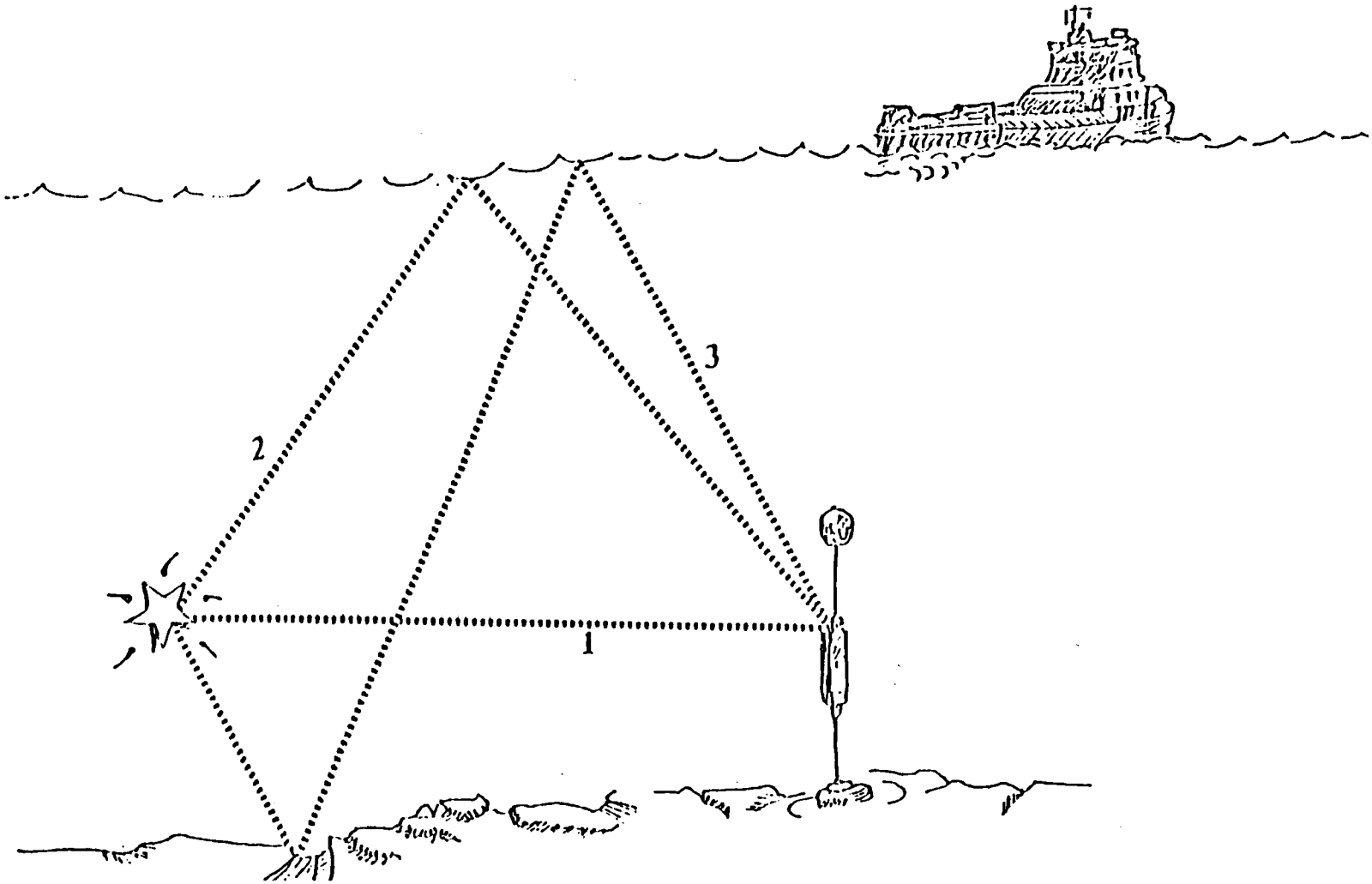

Figure 9. Schematic diagram of three water waves used to determine the shot depth and shot-receiver offset. The topography of this site, although not ideally flat, is smooth enough to enable interpolation of water depth, to determine the depth where the third water wave interacts with the sea floor.

three water waves is shown in Fig. 10. These different paths are the direct water wave, the wave reflected off the sea surface, and the wave first reflected off of the seafloor, then from the sea surface to the recording instruments. The travel times of the three different waves paths were determined by ray tracing from a densely spaced grid of assumed shot locations. The differences of travel time of the three different water waves are compared to the observed travel times to find the best fit of the shot depths and the shot-receiver ranges. By this method, the travel times of the direct water waves were determined from the best fitting of shot depths and shot-receiver ranges.

A bathymetric chart (Fig. 8) has been constructed from echo-sounding records collected during the cruise. The bathymetric chart reveals the bathymetry of this area in the upper Monterey Fan varies by about 100 meters over the 12km length of the refraction profile. To increase the accuracy of tracing the doubly-reflected water wave path, the depth of the bounce point on the sea floor was determined by interpolating the countours at the calculated horizontal position. A quality check was done by comparing the resulting shot depths and shot-receiver ranges of the same shot from different receivers, revealing the accuracy of the ray tracing method. The average difference between shot depths for any one shot is less than three meters, and the maximum was less than six meters. The maximum difference is still within the resolving power of the digital sampling interval (0.005 s).

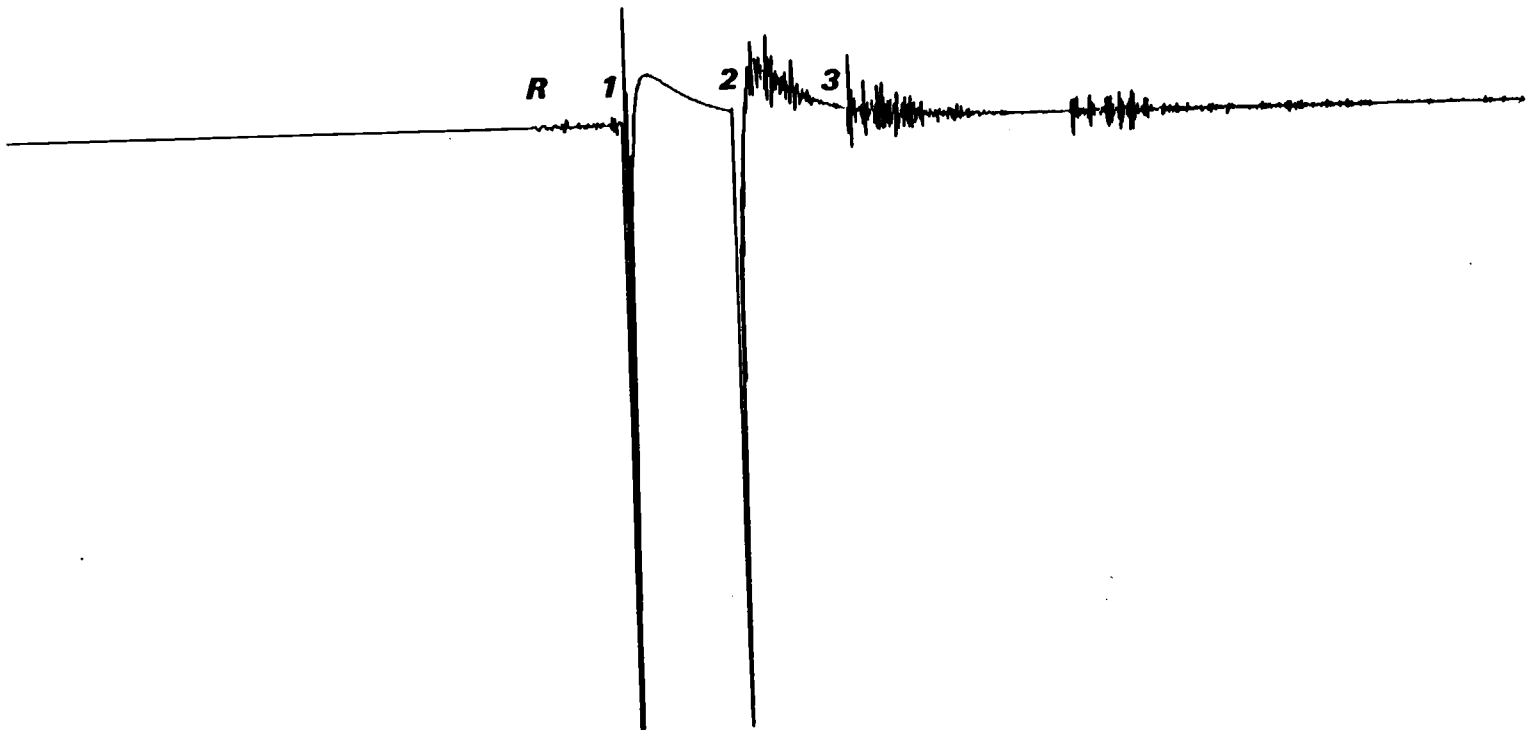

Figure 10. A sample seismogram from the Monterey Fan set. The water waves (1,2 and 3) correspond to the arrivals, shown in Fig. 9. The amplitudes of these water waves were too large to record linearly. The refraction wave (R) is the wave refracted from the subbottom structure.

DATA ANALYSIS

Record Section

Before reducing the raw data to the datum plane (the sea floor), we must determine the phase velocity of each returning wave . From the record section (Fig. 11), a clearly defined first arrival branch and several coherent secondary arrival branches were noted. Based on a radial cross section of the Monterey Fan (Wilde et al., 1978), which nearly passed over the upper Monterey refraction site, the maximum thickness of the sediment layer is about 2 km (Fig. 12). Shor et al. (1971) presented a nearby refraction profile (FF7), located 80 km west of the refraction site, with a basement layer with velocity 4.72 km/s and a 1.3 km thick sediment layer with a constant assumed velocity of 2.15 km/s. From both previous studies, a two layer model seems to be appropriate for the study area. To ensure the identification of the travel time branches, extreme care was taken. First, we compared the travel time curve of the first arrivals for the upper Monterey Fan with the curves of the Bengal Fan and the Nicobar Fan (Fig. 13). The Monterey Fan travel time curve crossed over the Bengal Fan curve at 5.5km range. The short-range data, which lie above the travel time curve of the Bengal Fan and the Nicobar Fan, imply low velocities and velocity gradients in the upper part of the Monterey Fan. The first two data points with low phase velocities in the travel time curve show poor fitting with other data with higher phase velocities; moreover, both the anomalous behaviors of the travel times and the amplitudes imply that the first two data points may not belong to the same travel time branch as the others. As we closely examined those seismograms from 5.5km to 9km, we found very coherent secondary arrivals, as pointed out in Fig. 11. Based upon the high quality

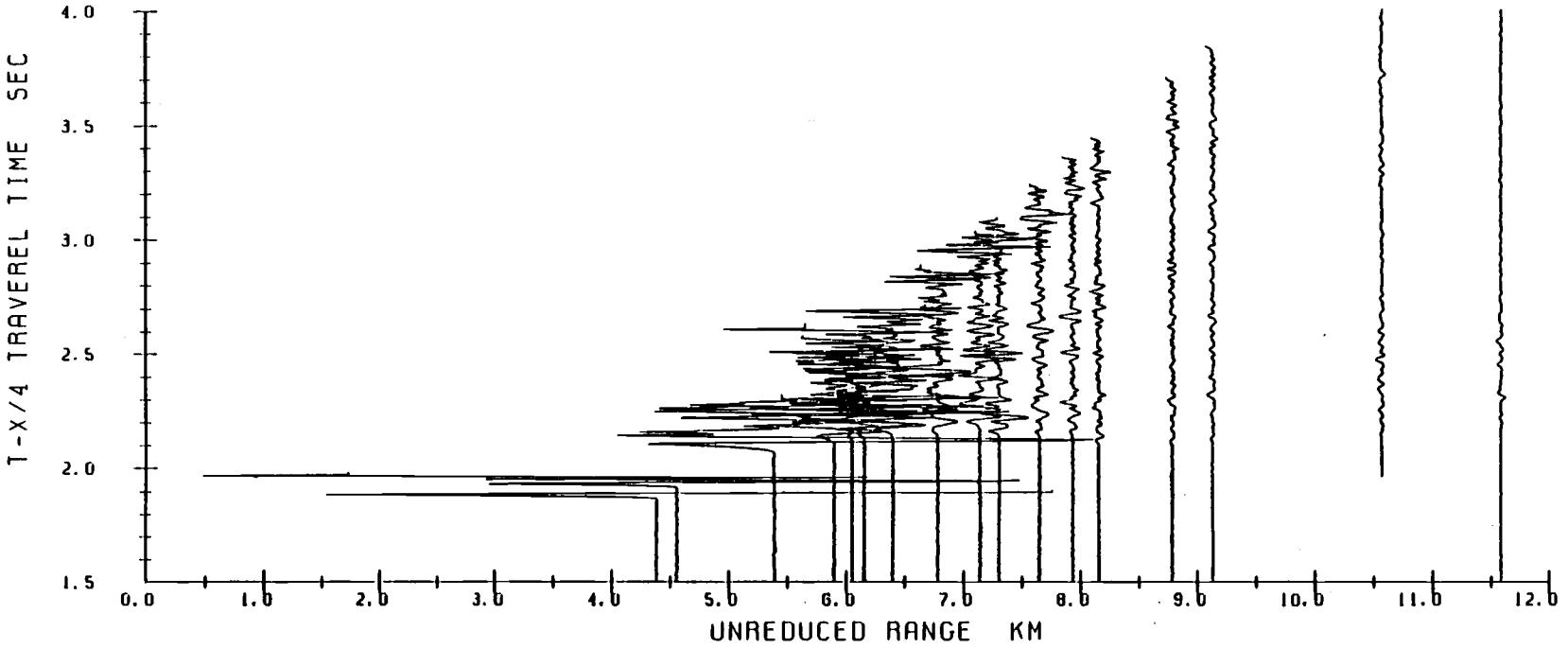

Figure 11. Record section with true amplitudes, reduced at a velocity of 4 km/s. A total 17 seismograms were recorded with refracted arrivals.

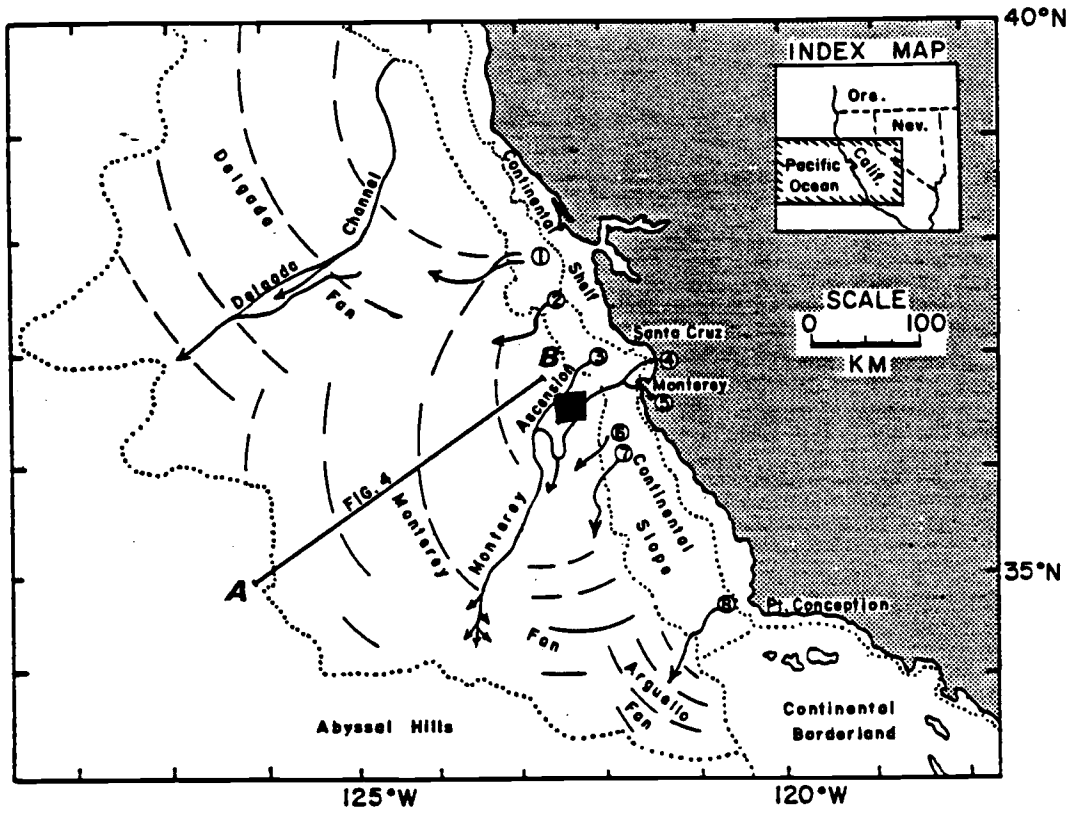

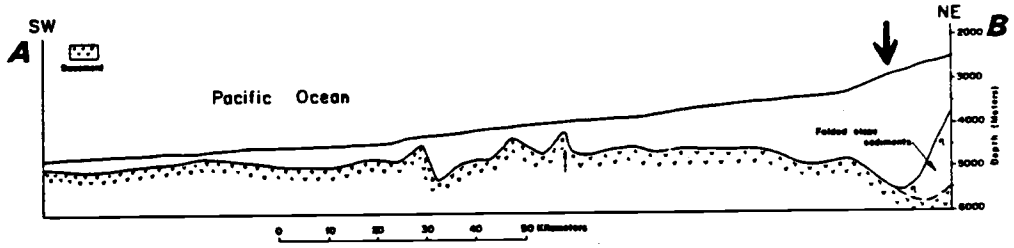

Figure 12. Location and diagram of radial cross section of the Monterey Deep Sea Fan (From Wilde et al., 1978). The thickness of fan sediments is calculated assuming a sediment velocity of 2 km/s. The arrow in the profile indicates the parallel position with respect to the refraction site. The upperpart is sediment structure and the lower part is acoustic basement structure.

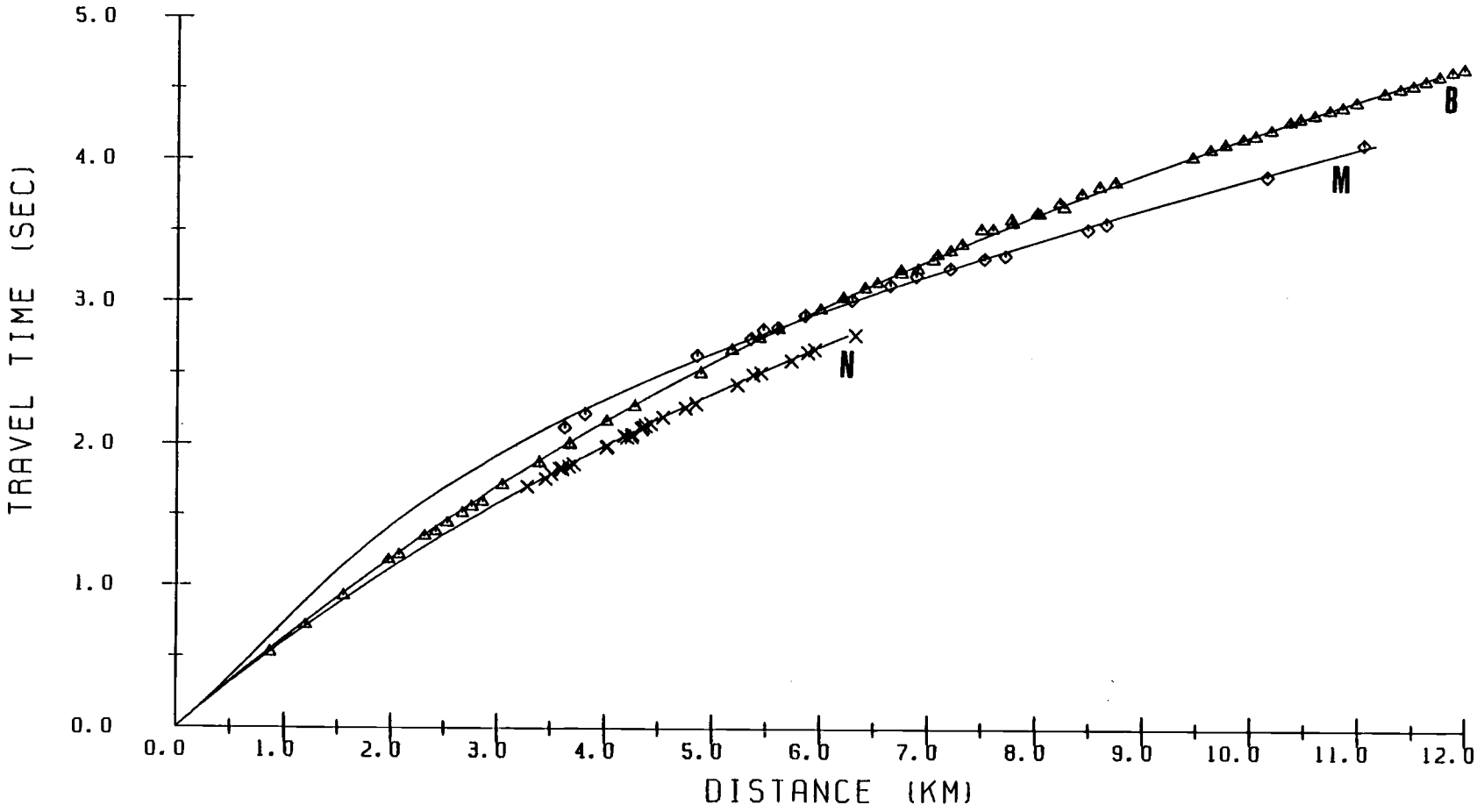

Figure 13. Travel-time plots of first arrivals, with polynomial regression curves, from the Bengal (B), Nicobar (N) and Monterey (M) data sets.

of the record section and the good coherency from shot to shot, the identification of the secondary arrivals could be accomplished. Examination of the phase velocity of the secondary arrivals reveals this branch may be the rays returned from the deeper sediment structure. A forward modeling method, which can refine the picks of the arrivals from the deep sediment layer, was used to calculate a synthetic travel time curve. The velocity model used in this forward calculation was the Bengal Fan velocity model which was reduced to 70% of its original values to match with the observed travel times of the first two sediment arrivals, which are at the shorter range than the basement arrivals in the Monterey Fan. The result shows the calculated travel times are almost exactly the same as the times of the first and secondary sediment arrivals (Fig. 14).

The Whispering Gallery Phases

Strong and coherent waves, coming slightly before the direct water waves, were noted as an unusual event. The low phase velocities and the strong amplitudes suggest that these waves may come from a typical shallow fan structure, which has a high velocity gradient. The reflected multiple-paths refraction waves were proposed to explain this unusual phenomenon. The waves travel within the shallow part of the sediment structures and reflected off the sea floor interface once, twice or more, as shown in Fig. 14. Some similar kind of phenomenon had been noticed and recognized as whispering gallery phases by Rayleigh (1910). Rayleigh introduced the whispering gallery effect to explain how sound waves propagating efficiently along the curved inside wall of St. Paul's Cathedral. Originally, the whispering gallery phases were introduced by a curved reflector, such as the inside of a dome. The waves propagate along a straight path in air

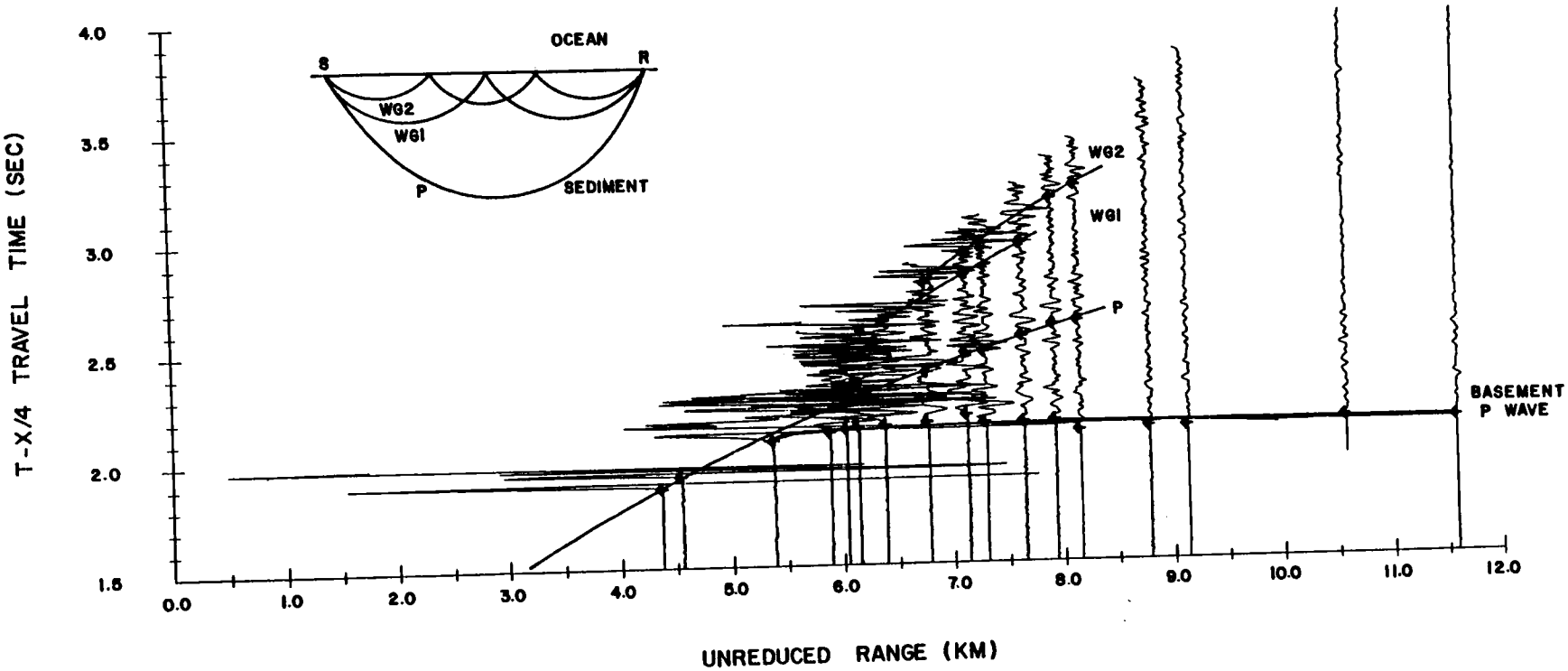

Figure 14. Record section with true amplitudes together with the calculated travel time curve from the forward model and travel time picks for the multiples (WG1, WG2) and the primary wave (P). (S) repesents the source and (R) represents the receiver.

and always bounce back due to the blocking wall. In deep sea fans, the structures are generally flat and layered, but the high velocity gradient characteristic of the uppermost sediment layer can refract many waves back to the surface within a shallow section as a wave guide. The deep-water explosive sources and the sea-floor receivers, provided seismograms with the high frequency (about 50 Hz) waves at a high sampling rate (200 samples/s), are the keys which allow the whispering gallery phases to be recorded and identified.

Menke and Richards (1980) discussed the analog of the whispering gallery effect which occurs within the earth. The whispering gallery phases events has been found aboundly in seismic studies for interfaces within the earth structures, such as in the crustal layer (Hill,1971a,b), the crust-mantle boundary (Menke and Richards, 1980), the core-mantle boundary (Choy,1977), and the inner-outer core boundary (Cormier and Richards, 1977). The wave composed of many multiples taken together is also known as the interference head wave (Cerveny and Ravinda, 1971).

The whispering gallery phases do occur at the sea floor interface. The high velocity-gradient sediment structure acts as the "whispering gallery" to refract rays back to the sea floor within several hundred meters of depth. The whispering gallery phases have been identified as follows. First, the systematic changes in amplitude and the good coherency from trace to trace of these high amplitude arriving waves reveal that these waves should return from a lateral homogeneous medium with smooth variation in depth. Secondly, the phase velocities of these coherent waves fall within the expected velocity range of the shallow sediment waves. Third, the variations in the amplitudes of these arrivals could be confirmed by the general trends of velocity gradients in the Bengal and Nicobar Fans. These strong amplitudes would be expected due to the high velocity-gradients

structure near the sea floor. Amplitudes of seismic waves are influenced by its geometrical spreading, transmission-reflection coefficients, and attenuation. In the frequency domain, the relationship between the amplitude and these factors can be expressed as follows:

$$A(Z,f)= A_0(f)\ [1/G(Z)]\ [T\text{-}R]\ \exp(-\pi f T Q^{-1}(Z)) \qquad (1)$$

where A(Z,f) is the amplitude of the refracted wave, $A_0(f)$ is the source function, 1/G(Z) is the geometric spreading coefficient, [T-R] is the total influence of transmission-reflection-conversion effects along the ray path, f is the frequency, T is the travel time, and $Q^{-1}(Z)$ is the specific quality factor to describe attenuation. The geometric spreading effect can be examined in more detail as Eq 9.44 in Aki & Richards (1980) and can be simply expressed as:

$$G(Z) \propto |\partial X/\partial p| \qquad (2)$$

where p is the ray parameter. Therefore, the amplitude ratio can be expressed as follows:

$$A(Z,f)/A_0(f) \propto |(\partial X/\partial p)|^{-1/2} = (\partial p/\partial X)^{1/2} \qquad (3)$$

where Δ presents the shot-receiver range and p is the ray parameter. The ray parameter, p, which is constant along a raypath, can be calculated as $\partial T/\partial X$, which equals the inverse of apparent velocity, V_a. The value of $\partial X/\partial p$ can be measured from the travel time curve, as the curvature $\partial^2 T/\partial X^2$.

It can be evaluated analytically from the velocity gradient structure. Noting that

$$\partial p/\partial X = \frac{\partial (1/V_a)}{\partial X} = \partial^2 T/\partial X^2 \qquad (4)$$

the apparent velocity can be evaluated in a horizontal layered structure with constant velocity gradient, dV/dZ, as follows:

$$V_a = \int_o^Z dV/dZ \; dZ \qquad (5)$$

In a laterally homogeneous and vertically smoothly-varying layer within a typical sediment structure in deep sea fans (except the channels), the horizontal distance of a ray path is proportionally increased as the penetration depth of the ray path increases. Therefore,

$$A(Z,f)/A_o(f) \propto dV/dZ \qquad (6)$$

The velocity gradient ($\partial V/\partial Z$) is directly proportional to $\partial X/\partial p$. In a high velocity gradient structure, the geometrical spreading effect will be anomalously low due to the small geometrical spreading coefficient, 1/G(Z). Furthermore, the over-lapping of different modes of whispering gallery phases will sum up all the amplitudes components and result in anomalously high amplitude waveforms. The rapid decrease of velocity gradient in depth will result a sharp reduction of amplitudes. This rapid

reduction of amplitudes was noted as these whispering gallery phases propogate to farther ranges. This approach was confirmed by forward modeling results. The same velocity model, a reduced 70% velocity-depth function of the Bengal Fan site, was used to make the arrival times of the various whispering gallery phases. The calculated travel time curve was a rather good match with our original picks of these coherent waves. The modes of these waves in the whispering gallery phases were also identified by this calculated travel time curve (Fig. 14). The results show that a total of eight multiple arrivals can be picked with confidence, three of these are double multiples and five are triple multiples. The entire usable data set for the Monterey Fan consisted of fifteen basement arrivals and sixteen sedimentary arrivals with eight primary (two first arrivals and six secondary arrivals), three double multiples, and five triple multiples.

Wave Path Correction

An iterative procedure with a fourth order polynomial, X(T), was used to reduce the raw data to the sea floor by tracing the ray path through the water column and removing both the distance and travel time due to the water path from the raw data. This procedure requires the knowledge of the phase velocity for each arrival. The iteration started with reasonable estimates of these phase velocities to calculate the reduced travel times and ranges. The fourth order polynomial was forced to pass through the origin, T=0, since the data were reduced to the sea floor. The polynomial is:

$$X = A_1 T + A_2 T^2 + A_3 T^3 + A_4 T^4 \qquad (7)$$

where X is the reduced shot-receiver range and T is the reduced travel time.

The aim of the regression was to obtain the estimates of the phase velocity of each arrival. The waves traveling as whispering gallery phases need special care in this analysis due to their different modes. Each reduced travel time and range data were divided by its mode to form the reduced signal pathway travel time and range data for obtaining the estimates of the phase velocities from polynomial regression. By taking the derivative of the regression function, the slope was found for each T_i; i.e.

$$V_i = (dX/dT)_i = A_1 + 2 A_2 T_i + 3 A_3 T_i^2 + 4 A_4 T_i^3 \qquad (8)$$

where V_i is the estimated phase velocity for the data point, T_i. The slope at origin, (T=0), should yield the estimate of the sediment velocity at the sea floor. The velocity V_i was used to reduce the raw data to the sea floor again. In every iteration, the reduce travel time and range data were calculated from the raw data with the calculated estimates of the phase velocity of each arrivals and divided by its mode; then, a new estimate of the phase velocity of each arrival was evaluated from the derivative of the polynomial regression. The errors in estimating the phase velocity will be examined in inversion process. This entire process was repeated until the residual errors were minimized. Meanwhile, the topographic effect of the sea floor was eliminated by calculating the depth of the sea floor where the ray entered from the estimated phase velocity. The reduced travel time and distance data are now ready for estimating the velocity structure.

MODEL

Sediment Structure

The modified tau-zeta linear inversion technique was applied to convert the reduced travel time data to a velocity-gradient versus depth function. The full derivation of the tau-zeta linear inversion is shown in Appendix I. This technique has been successfully used on oceanic crust (Stephen and Harding,1983) and marine sediments in both the middle Bengal Fan (Dorman and Jacobson,1981) and the Nicobar Fan (Jacobson et al.,1984). Because of the assumption of constant velocity-gradient layers, the travel time curve must show obvious curvature to reflect the existence of velocity gradients. The data from the Monterey Fan do show curvature of the travel time curve in the record section (Fig. 11 and 13). From the record section, the arrivals were identified and grouped into sediment refractions and basement refractions. The sediment refraction arrivals, composed of the primary and the multiple waves, were reduced to the sea floor datum by the wave path correction process. The final fourth order polynomial regression function provided the estimated phase velocity of each arrival, the inverse of slowness. The covariance matrix of the regression coefficients was used to calculate the covariance matrix of each estimated phase velocity. Due to physical reasons, the fourth order polynomial function was forced through the origin, T=0. The slope at T=0 was constrained by the knowledge of the surface sediment velocity, which is important in constraining the shallow velocity structure. If the polynomial regression function is constrained at the seafloor by an incorrect value, the resulting velocity gradients are apt to be biased. This is an essential step, but our data do not contain any direct velocity measurement at or near the

sediment surface. Therefore, the seismic velocity of the sea floor was computed from the ratio of sound velocity in sediment to sound velocity at the bottom of the water column. This ratio is invariant for a given type of sediment and is 1.033±0.006 for sand-silt-clay (Hamilton, 1970). Using the equation from Wilson(1960), the bottom water sound velocity was calculated to be 1503 m/s from a hydrographic station located near the refraction station. The surface seismic velocity of the sediment, which was calculated by multiplying the velocity ratio (1.033±0.006) by the bottom water velocity (1503 m/s), is 1552.6±9 m/s.

Using the wave path correction with polynomial regression function, the data were reduced to the seafloor with consistent individual phase velocities within three or four iterations. The reduced data, T(P) and X(P), can be reparameterized into τ (T-PX) and ζ (T+PX) as described in Appendix I. According to the derivation of the tau-zeta inversions, the inverse velocity gradient (dZ/dV) as a function of slowness is the real solution of the tau-zeta inversion process. Both a high model resolution and a small solution variance are desirable to achieve a good solution; however, a trade-off relationship between them requires a compromise. The trade-off relationship was demonstrated and discussed by Bee and Jacobson (1984), who concluded that a constrained model with as many layers as observed data represents a satisfactory compromise between the model resolution and solution variance. The model layer boundaries correspond to the turning depth of each ray path . Therefore, a model with sixteen layers was chosen for the upper sedimentary structure since a total of sixteen rays that returned solely through the sediment structure was recorded.

Using the tau-zeta inversion method, the velocity gradient of the upper Monterey Fan were found to be 0.875 s^{-1} at the seafloor and gradually

decreased to an asymptotic value of 0.590 s^{-1} at depth (Fig. 15). The velocity-depth function can be obtained by integrating the inverse velocity gradient with respect to the slowness, as shown in Eq.(A17) in Appendix I. In the velocity-depth function, the deepest propagating wave within the sediment has a velocity of 2.6 km/s and bottomed at the depth of 1.617 km. Since the inversion scheme is linear, the data covariance matrix is readily mapped into the convariance matrix of the final solution. The variance of the velocity-depth function was calculated using Eq. (A18) in Appendix. The 95% confidence bounds are shown for the velocity depth function (Fig.16). The solution has a chi-square value of 23 with 32 data points and 16 parameters. According to the "important n of data" as Eq.(A15) in Appendix I, the zeta data show 91.8% contributing to the solution and the reminder belong to the tau data. Therefore, the solution and the error bounds of the velocity depth function are mostly constrained by zeta, which is consistent with the observations from Dorman and Jacobson (1981) and Jacobson et al.(1984). When calculating the error bounds of the velocity depth function, the second term in Eq. (A18) in Appendix, which is due to the errors of the bounding velocities of each layer, is the most dominant term.

Acoustic Basement Structure

"Stripping" Scheme

Given the sediment velocity model, we now wish to construct the velocity model of the transitional zone between the sediment and basement layers and to extend the velocity structure downward. The same scheme as in the sediment analysis can be used to obtain the basement velocity model. Refraction interpretation often involves a "stripping scheme which

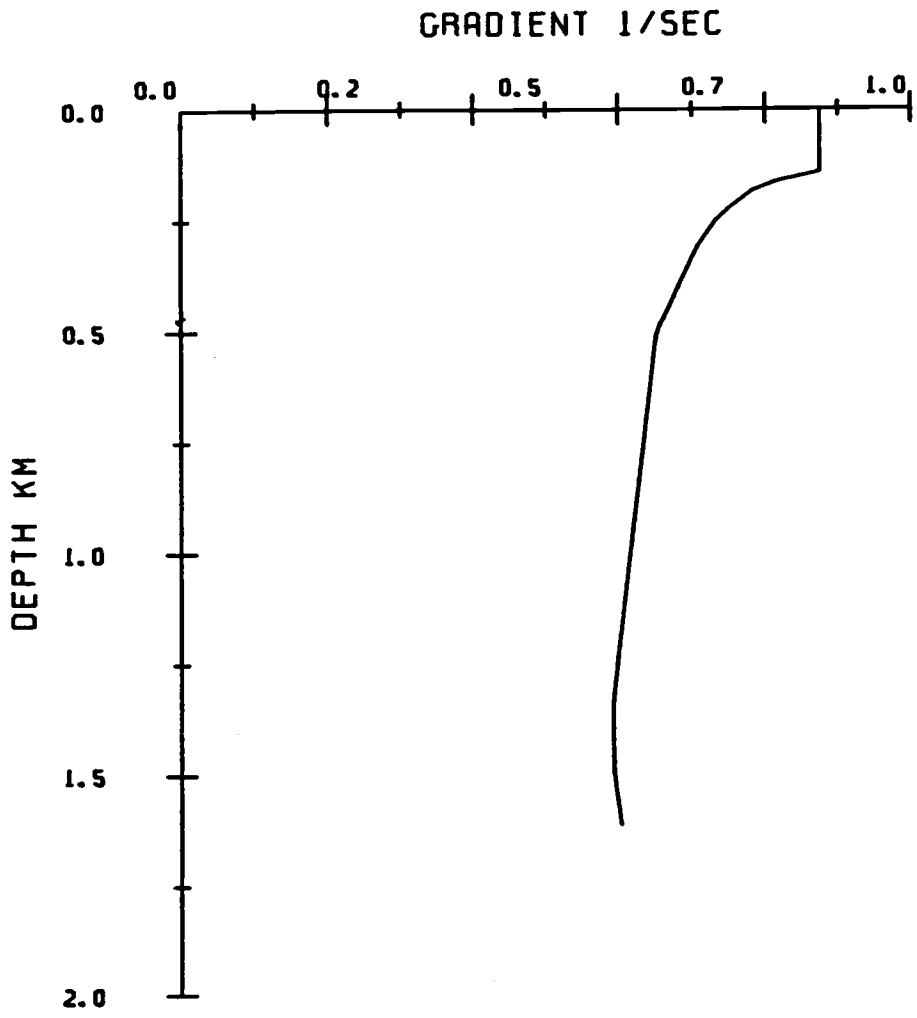

Figure 15. Velocity gradient versus depth for the Monterey Deep Sea Fan station with a value of 0.875 s^{-1} at the sea floor and an asympotic value of 0.590 s^{-1} at depth. A slight increase of the velocity gradient at the base of the sediment layer may indicate the progradation of the Monterey Deep Sea Fan.

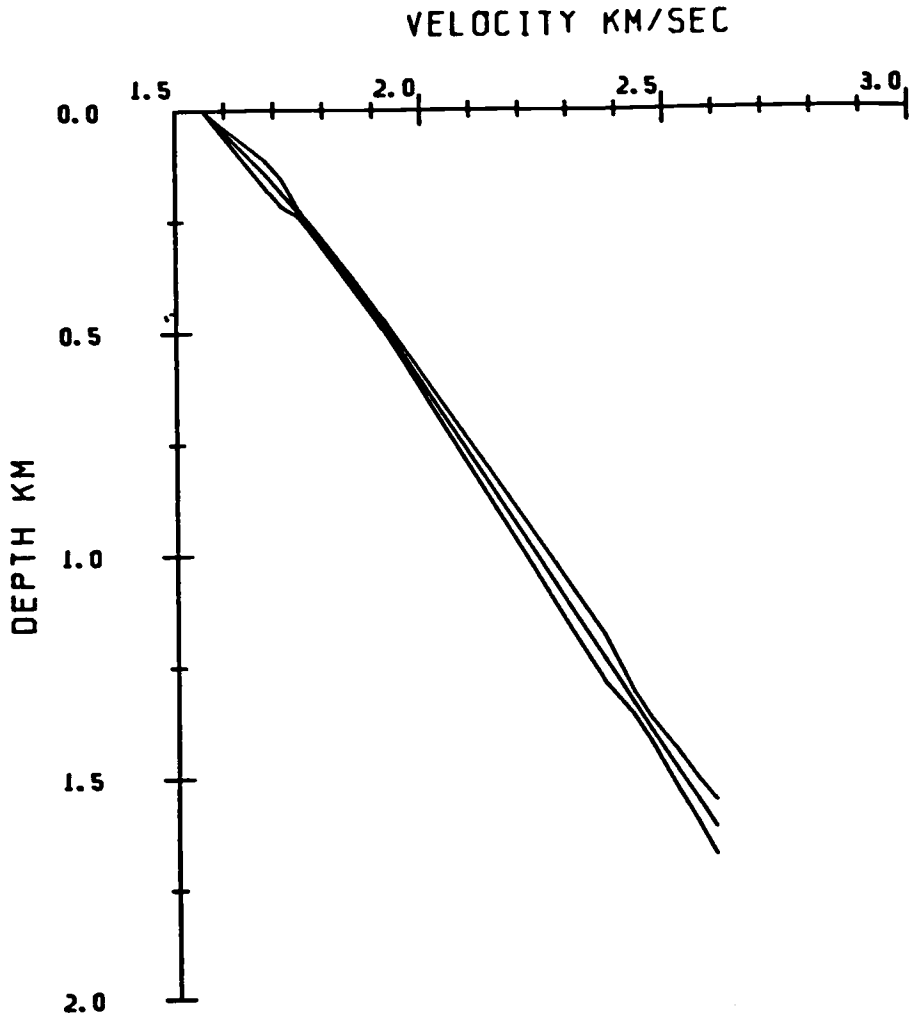

Figure 16. Velocity versus depth for thr Monterey Deep Sea Fan station with an assumed sea floor velocity of 1.557 km/s increasing to 2.6 km/s at 1.6 km depth. The upper and lower bound are 95% confidence bounds.

is essentially the removal of one layer at a time. In this method the raw data for the deeper refractors are adjusted to the bottom of the known structure. This adjustment is the same as the wave path reduction in the sediment layer, which substracts the travel times and ranges along the paths from the original shot point down to the original receivers. The new travel time curve is now solved for the deeper refracting layer after which the upper layer can be stripped off and the same inverse process can be applied. Following the typical travel time pattern of triplication, the deepest sediment determined layer can not be the real deepest sediment layer; therefore, the polynomial regression curve should not pass through the origin. Several problems arose during this analysis. First, the phase velocity of the first basement arrival could not be estimated confidently due to "the problem of polynomial regression". The problem of polynomial regression happens when the regression polynomial curve does not pass through the origin. The regression curve tends to drop below the time axis due to the lack of constraint in the short-range region. Therefore, the estimated phase velocity, the inverse of the slope, tends to be very small for the first data point due to the sharp increase of the slope. Secondly, no information concerning the depth of the discontinuity between the sediment and basement layers was available. Third, the uppermost or surface basement velocity is unknown at this stage. All three problems needed to be solved before the tau-zeta inversion technique can be applied to analyze the entire velocity structure.

For the sedimentary refracted arrivals, the data are fitted with a fourth order polynomial function, passing through the origin, to obtain estimates of phase velocities. For refacted arrivals propagating within the acoustic basement, the regression curve should not pass through the origin because

the data have not been reduced down to the top of the basement, but to the bottom of the known sediments. Several polynomial functions unconstrained at the origin were treated as the regression function, but negative intercepts always occurred. The phenomenon was due to the lack of short-range data. Consquently, the slope of the nearest data point, the inverse of the estimate of the phase velocity, would be biased by the problem of the polynomial regression function. Two methods were considered to avoid this problem. The first method, omitting the first datum point and using the estimated phase velocities of the remaining data points, was considered. However, omitting any datum point is not desirable especially since the first refraction datum is important in determining the shallow basement velocity structure. The second method, using a simple exponential function was considered, since it varied smoothly outside the range of the data. This linear exponential regression function (Eq.9) provided a rather good fit and yields confidence estimates of the phase velocities for the basement data. The regression function is shown below:

$$X = A_1 + A_2 T + A_3 \exp(T) \qquad (9)$$

where T and X are the travel time and shot-receiver range, respectively, reduced to the solved bottom of the sediments. An iterative procedure was used to reduce the data down to the bottom of the sediments until the estimated phase velocities become stable. The depth of the sediment-basement boundary was calculated from several assumed conditions and the knowledge of the delay time, tau, of the transitional layer.

We assumed that the transitional layer is composed of the deepest sediment layer below the turning depth of the deepest observed sediment ray path, the uppermost basement layer above the bottoming depth of the

observed shallowest basement ray path, and an interface layer which should be infinitesimal thin with infinite velocity gradient. First, we reduced the shallowest basement data point, having a phase velocity of 3.682 km/s, to the bottom of the known sediment structure, at 1.67 km depth. The intercept time, tau, constructed from the reduced range and travel time of the first basement arrival, is for a wave along a ray path which starts from the sediment bottom and travels downward, and then is returned from the bottoming depth of the first basement wave, the basement of the transitional zone. From the regression curve, the predicted tau was used instead of the observed tau, which showed an unstable value. The tau for a wave which traveled along such a ray path (from the transitional zone) with a slowness of 0.270 s^{-1}, is 0.048 s in two way travel. Three possible models for the transitional zone, as stated by Goodman (1983), are presented as follows:

First, assume that the bottom sediment velocity (V_S) of 2.602 km/s at 1.617 km continues to the discontinuity (the interface) and then jumps to the basement velocity V_b of 3.682 km/s as model 1 in Fig. 17. This transitional zone thickness is calculated from the delay time due to a homogeneous layer with a velocity of 2.602 km/s. The thickness of this homogeneous layer needed to generate a delay time, τ, of 0.0242 s, for a ray path with a slowness 0.2716 s/km is

$$H = \frac{\tau \quad V_S}{\cos\left(\sin^{-1} V_S/V_b\right)} = 89\text{m} \qquad (10)$$

This leads to a depth of the sediment-basement discontinuity of 1.706 km.

The second model assumes that a linear velocity gradient exists

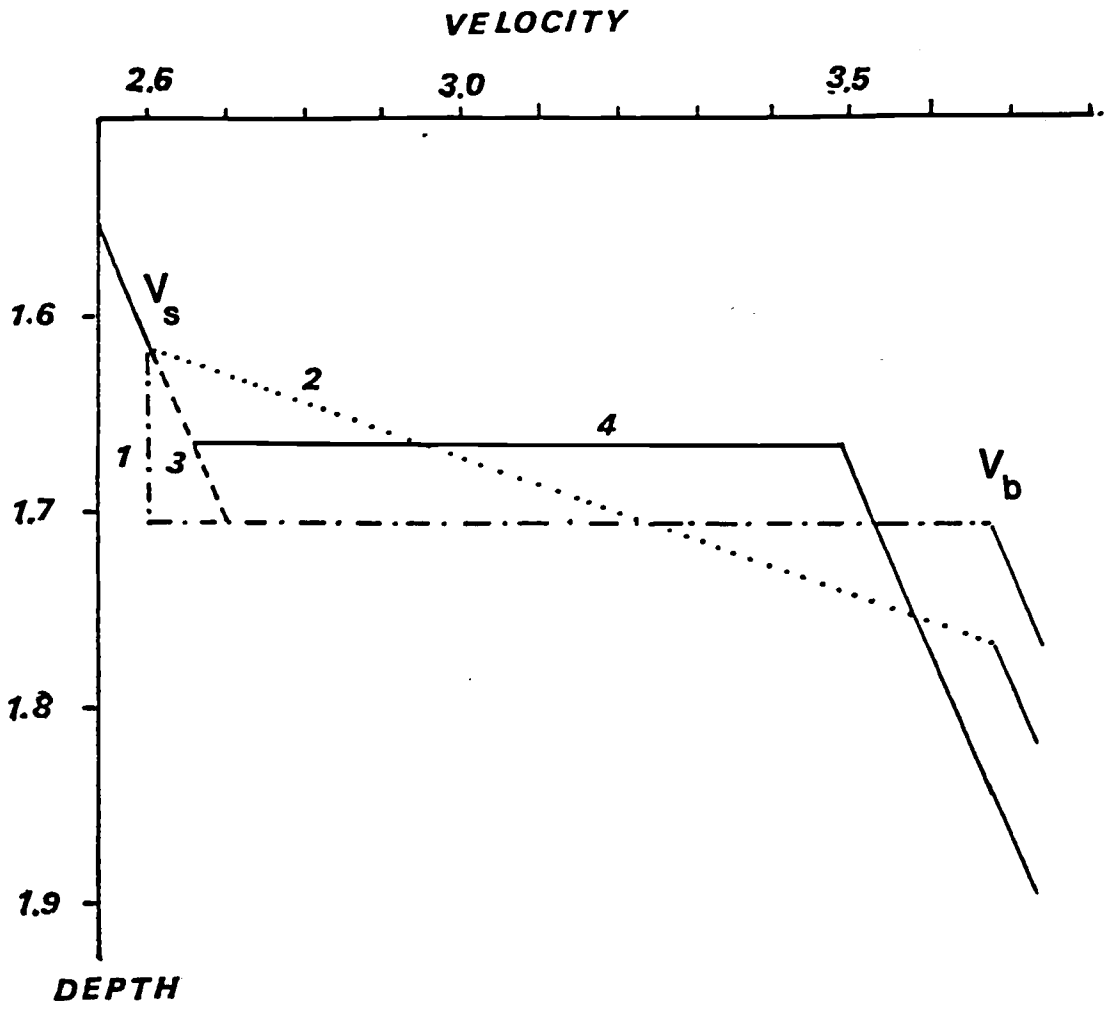

Figure 17. Models of the transitional zone with the constant velocity model (1), the constant velocity gradient model (2), the extended sediment velocity gradient model (3), and the sediment and basement extended model (4). V_s and V_b are the phase velocities of the last sediment and the first arrivals.

between the deepest sediment velocity V_S, 2.602 km/s, and the shallowest basement velocity V_B, 3.682 km/s as model 2 in Fig. 17. This is the case of calculating travel time and range for a constant velocity gradient layer. The calculations are as follows:

$$T = \ln \left[\frac{dZ}{dV} \frac{V_b}{V_s} \frac{(1+(1-p^2 s^2)^{1/2})}{(1+(1-p^2 V_b^2)^{1/2})} \right] \qquad (11a)$$

$$X = \frac{dZ}{dV} \ln \left[\frac{(1-p^2 V_s^2)^{1/2}}{p} - \frac{(1-p^2 V_b^2)^{1/2}}{p} \right] \qquad (11b)$$

so that

$$\tau = T - pX = \frac{dZ}{dV} \left[\ln \left(\frac{V_b}{V_s} \left(1+\frac{V_s^2}{V_b^2}\right)^{1/2} \right) \right] - \left(1-\frac{V_s}{V_b^2}\right)^{1/2} \qquad (12)$$

Using Eq (12), the velocity gradient (dV/dZ) was found to be 7.2 s^{-1}. This yields a transitional zone thickness of 150 m. The depth at the base of the transitional zone is at 1.767 km.

The third model assumes that the velocity gradient just above 1.617 km depth continues down to a discontinuity at which the velocity jumps to the first observed basement velocity V_b as model 3 in Fig. 17. The velocity gradient from a depth of 1.2 km to just above 1.617 km was found to be 0.59 s^{-1}. This model can be solved iteratively using Eq. (11a) and Eq. (11b), resulting in a thickness of 91m for the extended sediment layer and a velocity just above the interface of 2.656 km/s. The discontinuity depth in

the boundary is 1.708km.

Using both tau and zeta of the entire basement data set, a fourth transitional zone was proposed. This transitional zone of this model includes two unconstrained layers and one interface; one upper layer consists of sediment ranging in depth from the bottoming depth of the deepest sediment ray path to the discontinuity and the other layer constists of basement from the discontinuity to the bottoming depth of the shallowest basement ray poth. This model assumes that the velocity gradient just above the 1.617 km depth continues down to the discontinuity at which the velocity jumps to the uppermost basement velocity V_{b1}. This basement velocity increases with an assumed velocity gradient value, $(dV/dZ)_{b1}$, from the uppermost basement velocity V_{b1} to the basement velocity, V_b. The assumed velocity gradient $(dV/dZ)_{b1}$ can be used from a "trial and error" method. This procedure was continued until a consistent velocity gradient was obtained. The results from the generalized inversion scheme provided a good indication of the range of the first basement velocity gradient. Basically, two unconstrained layers are calculated, one is the extended sediment layer and the other assumed basement layer extends from the discontinuity down to the first basement ray's bottoming depth. After several adjustments in $(dV/dZ)_{b1}$, the results give a thickness of 50 m for the deepest sediment layer and 80m for the uppermost basement layer. The velocities at the discontinuity are 2.632 km/s at the base of the sediment and 3.401 km/s at the top of the basement. The depth for this discontinuity is 1.625 km.

The velocity-depth functions for these four models, describing the sediment basement transitional zone, are shown in Fig.17. The constant velocity model and the continuous sediment velocity gradient model yield

similar results for the depth of the boundary. However, any model which does not consider the existence of a surface basement velocity is physically unlikely. The first arrival of the basement data, which is treated as the uppermost basement velocity in the first model, cannot belong to a wave long a ray path which just grazes the basement. The fourth model is more reasonable from a physical perspective and has consistent velocity gradients with the rest of the velocity solution near the transitional zone.

We now have the boundary condition between sediment and basement layers, so the raw basement data can be reduced to the depth of the boundary and be ready for the tau-zeta inverse method. A similar methodology to that used for the reduced sediment data was used for the reduced basement data. The same inversion scheme was used to construct the velocity depth function of basement structure. The sediment and basement velocity depth functions are presented in Fig. 18. The deepest basement arrival shows a velocity of 5.738 km/s with a depth of 4.246 km.

General Scheme

The above method solves for the sediment velocity structure first, then the transitional zone, and finally the basement velocity structure. The refracted waves which have propagated within the basement also contain some information of the sediment structure. Therefore, we should invert the entire data set into a complete velocity-depth solution, called the general inversion method. We have expanded the tau-zeta inversion program to handle both sedimentary and basement data together with a three-layer transitional zone. The three-layer transitional zone is the same as in the fourth transitional zone model, i.e. the bottom sediment layer, the top basement layer, and an interface layer, which is used to test the validity of

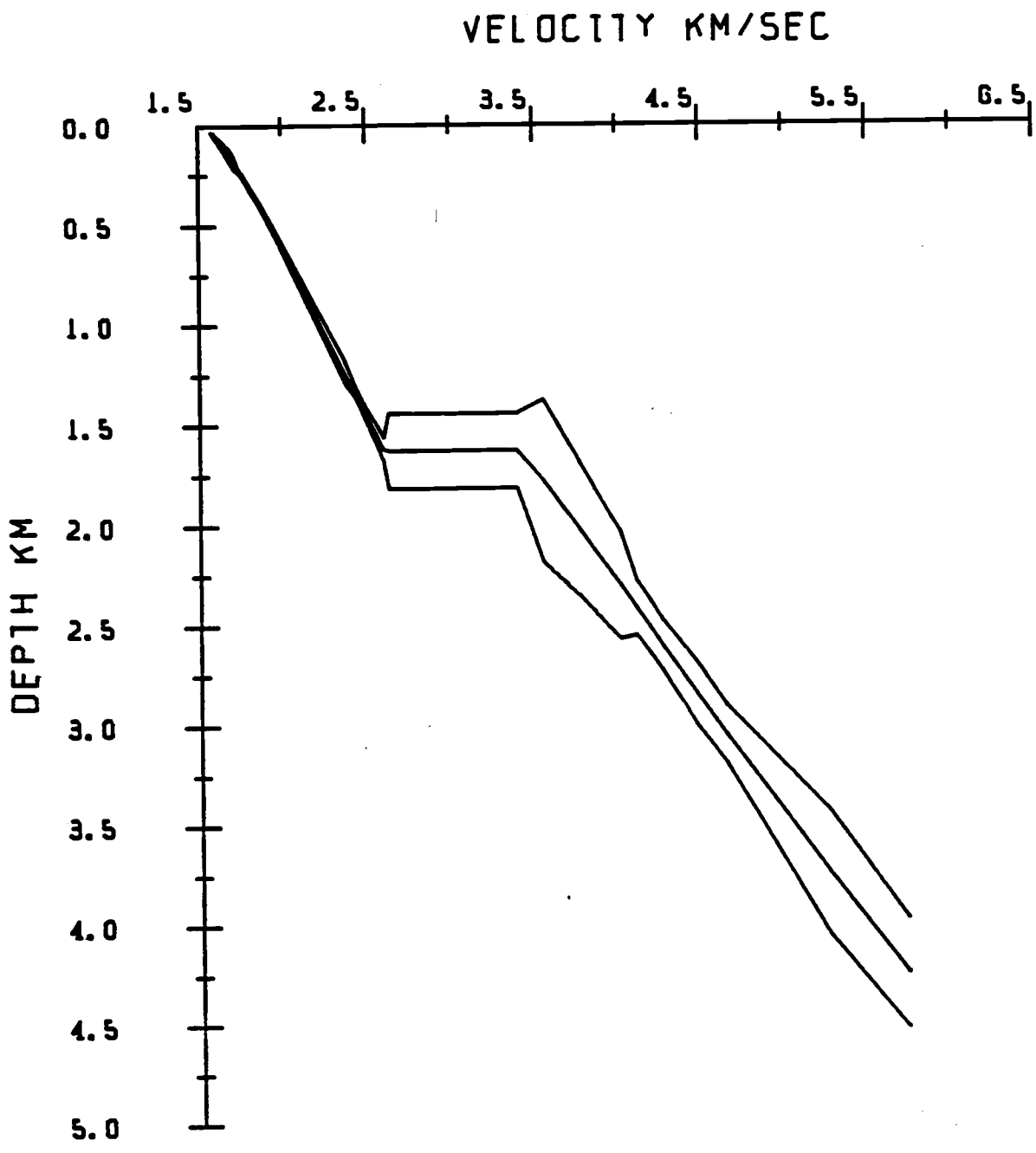

Figure 18. Velocity structure of the entire structure, solved by the "stripping" scheme with a boundary at 1.625 km depth.

the model. First, all raw sediment data were reduced to the seafloor with a fourth- order polynomial function as in the previously sediment part calculation Eq. (7). Similarily, the raw basement data was reduced to the seafloor with a simple combined exponential function as in Eq. (9). The same regression functions used previously in each layers were used here to keep consistency of the estimated phase velocities.

Three important checks help us to define the best solution. These are the continuity of the sediment velocity gradient above the boundary, the continuity of the basement velocity gradient below the boundary and the infinite velocity gradient between the sediment and basement layers. A small problem arose while determining the transitional zone: three extremely small eigenvalues caused an unrealistic velocity gradient of the interface. After adjusting the cut-off point of the eigenvalues by raising the allowable eigenvalue ratio to 0.001 in the inversion process Eq.(A12), a stable and reasonable velocity gradient structure was obtained. Velocities at the discontinuity (1.582 km) were found to be 2.640 km/s at the bottom of sediment and 3.400 km/s at the top of basement (Fig.19).

The validity of the model was indicated by both a high velocity gradient, 5438.0 s^{-1}, between the sediment and basement structures, and the continuous velocity gradients for both the sediment and basement layers. The 95% confidence bounds were calculated as Eq.(A18) and are shown in Fig.19.

Comparison of General and Stripping Solutions

A comparison of the resultant models of the general scheme and the stripping scheme is shown in Fig. 20. The 95% confidence bounds of the general solution are obviously wider than that of the stripping solution. The

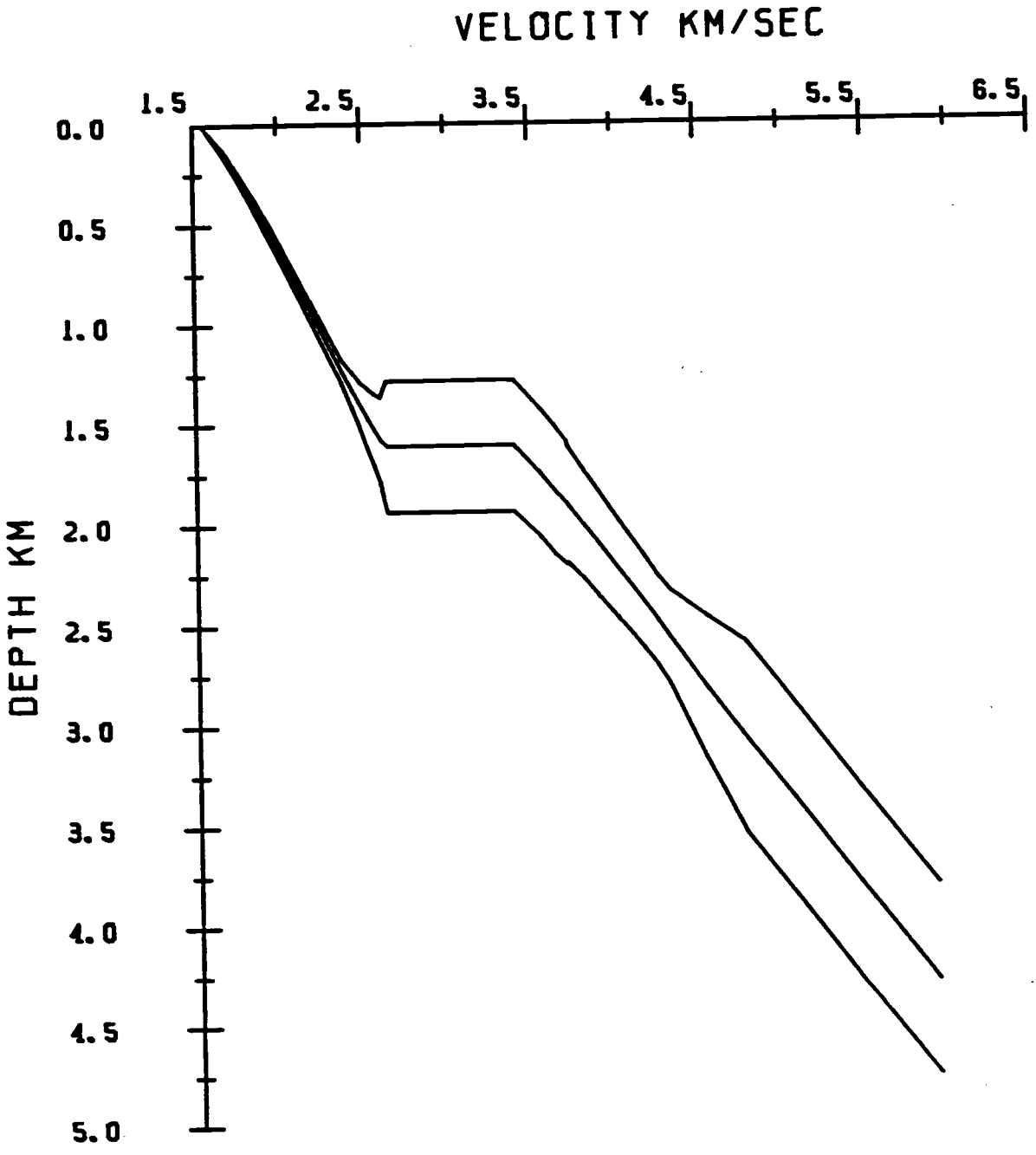

Figure 19. Velocity structure of the entire structure, solved by the general inversion scheme with a boundary at 1.582 km depth.

VELOCITY KM/SEC

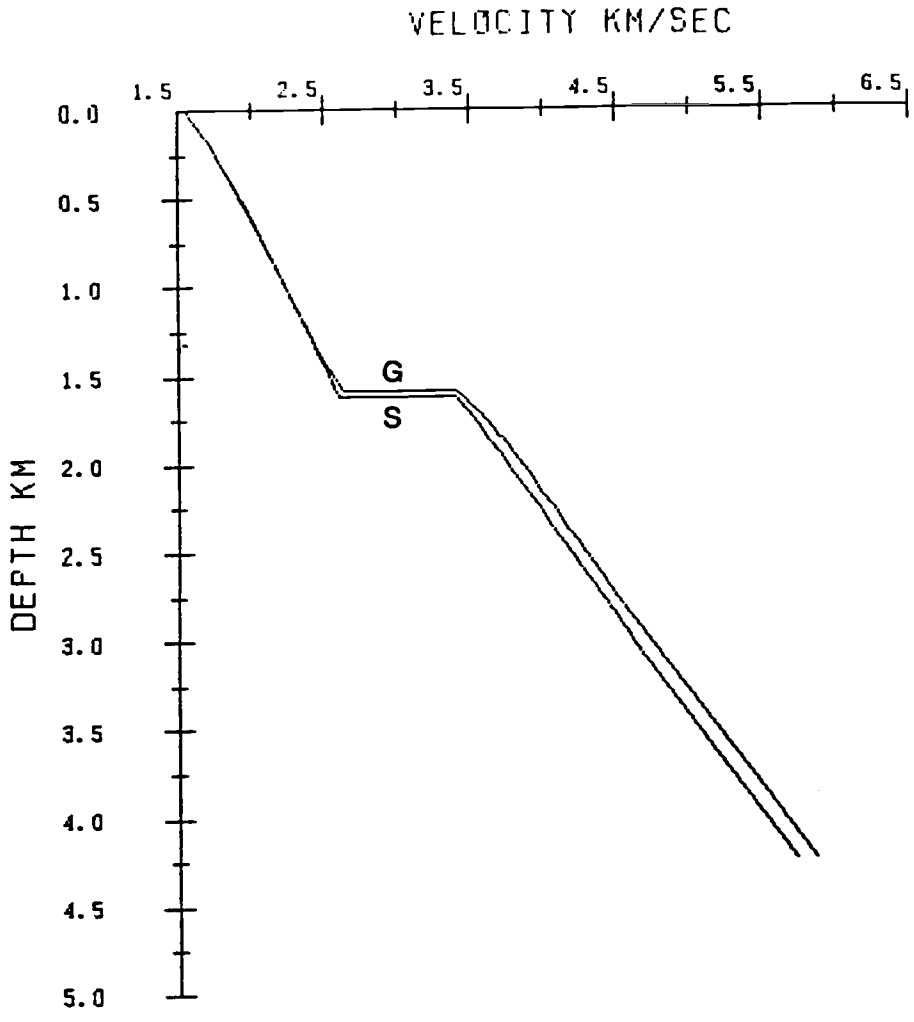

Figure 20. Comparison between the results of the models using the "stripping" scheme and the general inversion scheme. The velocity-depth function for the former scheme is labeled S and that for the later scheme is labeled G.

error analysis of the transitional zone in the stripping method is unsatisfactory. The general solution really provides a better estimate of the errors than the stripping result. In the general solution, the depths for this transitional zone are 1.575 km for the deepest sediment arrival, 1.582 km for the discontinuity and 1.710 km for the first basement arrival. The deepest basement arrival shows a velocity of 5.873 km/s at the depth of 4.249 km. The sediment structure of the general solution is slightly shallower than the previous solution of the sediment layer, solving purely by the sedimentary arrivals. This change may be caused by the additional information of sediment structure provided by these basement arrivals. The velocity structure of the basement from both the general and stripping schemes shows the similar velocity structure which has a lower velocity, 3.4 km/s, on the uppermost part of the basement than normal oceanic crust, about 4.0 km/s. A normal oceanic crust with several fractures and faults can result in a lower seismic velocity but the overlying sediments which have filled in those open spaces can raise the velocity near to that velocity typical of normal oceanic crust. A pre-fan continental rise sediment layer underlies the fan structure. Normark (1984, personal communication) drew the same conclusion from unpublished seismic data. The underlying oceanic crust of the Oligocene age was formed along the Pacific-Farallon spreading center, which died off the central California by the Late Oligocene (Atwater, 1970). Normark et al. (1984) pointed out that the Monterey Fan probably did not begin to develop until the latest Oligocene or Early Miocene time when turbidity currents from the California margin could first the reach fan area. Therefore, these pre-fan sediments should
have been deposited after the oceanic crust was formed and before turbidites began to be deposited on this area.

PHYSICAL PROPERTIES

Several useful physical properties, such as density, porosity, effective pressure, and temperature, were derived from velocity and velocity gradient. Since the velocity gradient profiles from three different fan subunits are available, their physical properties can be compared to determine the characteristics of lateral variation on deep sea fans. The velocity gradients of seismic waves are affected by several major factors, such as porosity variations, temperature gradients, and degree of lithification (Hamilton,1978). The reduction of porosity with depth of sediments is caused by the increase of the overburden pressure as the younger sediments are deposited on the sea floor. Porosity is the key parameter to explain the velocity structure of sediments. All other factors are strongly related to porosity. For example, the thermal conductivity of marine sediments is dependent on the amount of water in sediments. Cementation between mineral grains begins when the grains are in close contact as the porosity decreases.

Porosity is defined as the ratio of the volume of voids (or pore space) to the total volume of a saturated sediment. The pore water expels out when the porosity is decreased by compaction and lithification effects. Compaction and lithification reduce the porosity by decreasing the amount of pore space through physical and/or chemical reactions. Hamilton (1979) pointed out that bulk modulus, rigidity and density of sediments are strongly dependent on porosity, and porosity is a more direct index to velocity than density. Jacobson et al. (1984) concluded that the porosity controls the vertical and horizontal changes in density, pressure, seismic velocity and attenuation. Overburden pressure, temperature and mineralogical changes

were examined and evaluated as a function of the increase of seismic velocity and depth (Hamilton, 1979). Overburden pressure was demonstated as having the most influence in determining seismic velocity. The load of additional sediment weight increases the overburden pressure and results in porosity reduction and change of frame bulk modulus. The overburden pressure, P, is the sum of the hydrostatic pressure in the sediment, P_h, and the effective pressure (also called the differential or intergranular pressure), P_e, so that $P=P_h+P_e$. Effective pressure is the sum of intergranular pressures, resulting from the buoyant weight of mineral grains, and is transmitted through the mineral structure. Hamilton (1979) discussed the individual overburden pressure effects on the elastic modulus for determining the wave velocity in both a qualitative and a quantitative sense. Using the results of compaction experiment of Cernock (1970) and the results of the hydropressure experiment of Laughton (1954,1957), Hamilton (1979) estimated that a 66% sound-velocity increase in the silty clays and turbidites within 500m of depth should be due to the compaction effect and a 2% increase due to the hydrostatic pressure.

The water content of marine sediments should be an equilibrium condition between the influx of water from the new sediments and the outflow of water due mostly to the compaction. Adding new sediments, such as silt with a high water content, can increase the water content in sediments. An area with high sedimentation rates may result in a higher water content structure than in other areas, for the newly deposited sediments will be covered by the new sediments before the equilibrium stage can be reached. Magara (1976) studied the water expulsion from a sand-shale interbedded model, a similar structure in the upper and middle fan subunits. Without adequate conduits (e.g. a high permeable vertical sand body or a fault), the pore water will move horizontally between the low

permeable shale layers under the overburden pressure.

Due to the lithology, facies, and sedimentation rates changes with time, a lateral and vertical, inhomogeneous velocity structure may result. To properly separate these effects is difficult. The velocity analysis of the seismic refraction profile actually yields a gross, average velocity-depth function rather than a precise velocity measurement as sonic logging. In essence, all of the effects from lithification, facies and sedimentation environment are averaged vertically. Using an empirical relationship between compressional wave velocity and density in marine sediment (silt,clay, turbidites) and sedimentary rocks (mudstones, shales) from terrigenous sources (Hamilton, 1978), a density-depth function can be derived from a velocity-depth function. The relationship used is shown in Table 1. The average porosity profile with depth can be calculated from the density depth relationship by the formula

$$\rho(Z) = \eta\,\rho_w + (1-\eta)\,\rho_g \qquad (13a)$$

so that

$$\eta = \frac{\rho_g - \rho(Z)}{\rho_g - \rho_w} \qquad (13b)$$

where ρ_g is the grain density and is assumed to be 2.78 gm/cm^3. ρ_w is the density of sea water and $\rho(Z)$ is the density at depth Z.

Jacobson et al. (1984) formulated a simple effective pressure calculation with the assumption that the interstitial water is free to move both vertically and horizontally. The equation for in situ effective pressure is

TABLE 1. An Emprical Relationship between Density and Compressional-Wave Velocity in Marine Sediment (Silt clay, turbidites)

Form of Relation	Condition
$\rho = 14.8\ V_p - 21.014$	$Z = 0$
$\rho = 1.135\ V_p - 0.190$	$V_p \leq 2.007$
$\rho = 0.917 + 0.744\ V_p - 0.080\ V_p^2$	$2.007 \leq V_p \leq 4.20$

From Hamilton (1978). The units of density (ρ) and velocity (V_p) are $^{g}/_{cm^3}$ and $^{km}/_{sec}$, respectively.

$$P(z) = g \int_0^Z [\rho(Z) - \rho_w]\, dZ \qquad (14a)$$

where g is the acceleration of gravity. The above equation can be rewritten in terms of the seismic velocity gradient, as

$$P(Z) = \sum_j \{ g \int_{V_{j-1}}^{V} [(\rho(V) - \rho_w) \quad [\frac{dZ}{dV}]_j]\, dV \} \qquad (14b)$$

where V_{lim} = Min(V_j, 1/p). Using Jacobson's assumption, we can eliminate the hydrostatic pressure in our calculation. This may not be a reasonable assumption since a highly impermeable layer can stop the vertical water transport, which is the same situation as the interbedded model in Magara's (1976) experiment.

The temperature versus depth function can be computed using the method from Hamilton (1979). A regression formula (Bullard, 1963) is used to calculated resistivity R (the reciprocal of conductivity), in the units of cm s ^{o}C/cal, from the water content, W, as a proportion of the net weight in marine sediment.

$$R = 168 + 678 * W \qquad (15)$$

The conductivity is obtained and used to estimate the thermal gradients-versus-depth function as TG=H/C, where TG is the thermal gradient, H is the heat flow in units of cal/cm^2 s X10^{-6} as HFU, and C is the thermal conductivity in the units of cal/cm s ^{o}C X 10^{-3}.

Due to the fact that heat flow was not measured during any of the three stations, the heat flow was estimated from the ages of crusts (Parsons and Sclater, 1977). The Monterey Fan was built on oceanic crust of Oligocene age (Normark et al., 1984); therefore, the mean heat flow was estimated to be 2.15 HFU. This estimate is very close to some nearby field measurements of about 2 HFU (Wilde et al., 1978). The heat flow on the central Bengal and Nicobar fans is estimated to be 1.6 HFU and 2.0 HFU according to the age of the underlain crusts. (Curray et al., 1982 and Sclater and Fisher, 1974). The temperature-versus-depth profile is found from the thermal gradient profile, as $T=T_0 + T\,G_i * D_i$, where T is the instantaneous temperature in ^oC at depth D in meters, T_0 is the sea floor water temperature and TG_i is the thermal gradient for layer i in $^oC/m$.

DISCUSSION

The velocity gradient and velocity profiles from the upper Monterey, middle Bengal, and lower Nicobar Fans show a remarkable morphologic similarity in the velocity and velocity gradient functions with depth but have significant differences in the values of the velocity gradient(s) at depth (Fig. 21 and 22). The coefficients of three polynomial regression functions is shown in Table 2, and the A_1 coefficient is actually the surface sediment velocity. The velocity gradient-depth functions show a typical vertical variation of deep sea fans, a high gradient near the sea floor and a rapid decrease to a constant value in an exponential fashion. The inflections of velocity gradient happen above 1000m of depth. This common variation implies similar physical property changes are occuring at all three deep sea fan sites, each of which represent each one of the three fan subunits. The asymptotic values of velocity gradients of the upper Monterey Fan, the middle Bengal Fan, and the Nicobar Fan are $0.59s^{-1}$, $0.68\ s^{-1}$,and $0.81\ s^{-1}$, respectively. Hamilton (1976) analyzed the samples from the DSDP site 222, in the Arabian Fan, and stated that between 300 and 600 m (porosity between 50% and 35%) the significant variations of the porosity may indicate the depth at which most thick sections of terrigenous sediments in the sea floor will become lithified. This observation help to explain the rapid variation in the shallow depths and a constant velocity gradient below a certain depth. Sediment porosity, which is normally very large near the seafloor, decreases with depth due to the overburden pressure and chemical diagenesis.

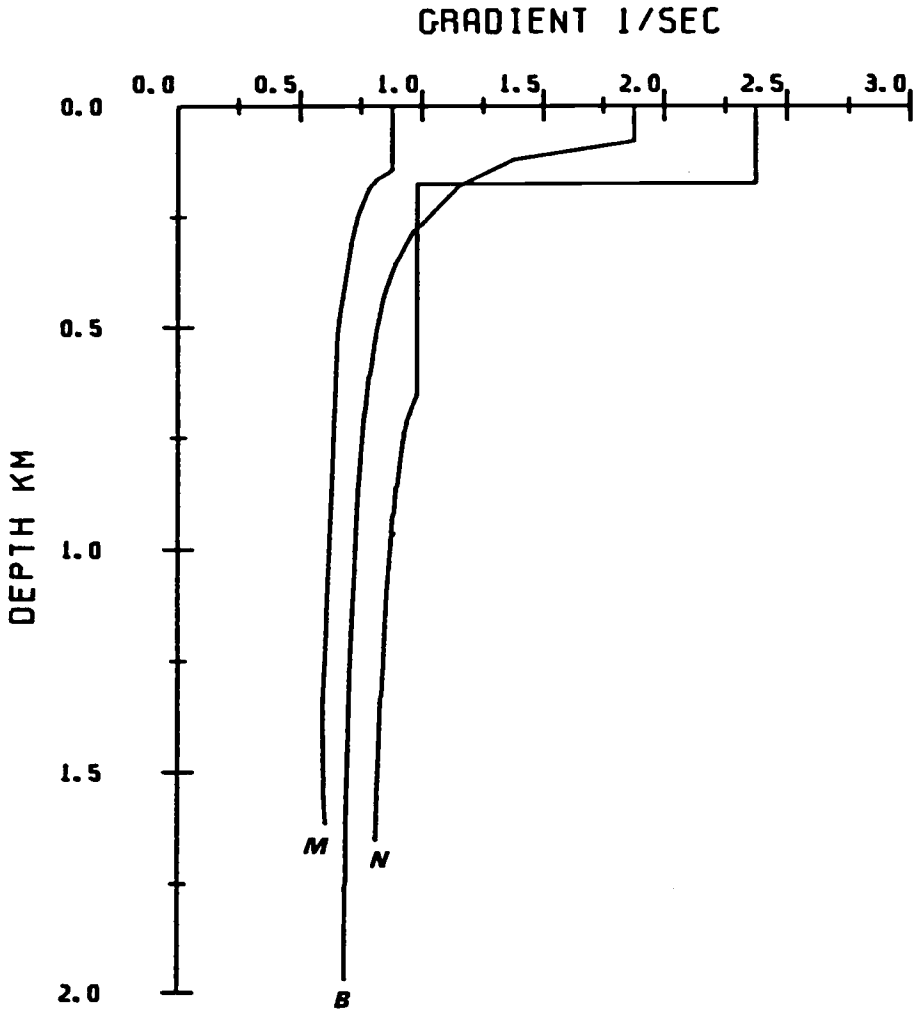

Figure 21. Velocity gradients versus depth for thr upper Monterey, middle Bengal and Nicobar Deep Sea Fan stations. Initial velocity gradients of 0.875 s^{-1}, 1.870 s^{-1} and 2.320 s^{-1} decrease to 0.590 s^{-1}, 0.670 s^{-1} and 0.810 s^{-1} at depth for the upper part of the Monterey Fan (M), the Bengal Fan (B) and the Nicobar Fan (N).

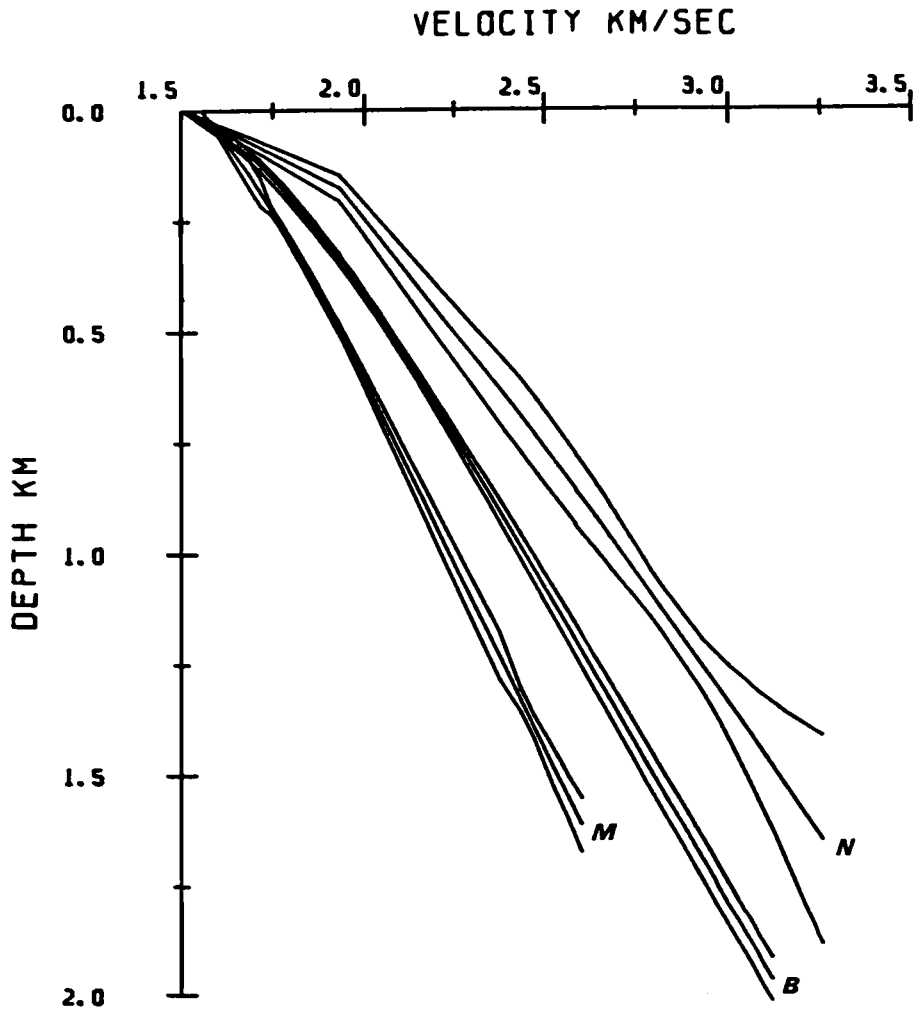

Figure 22. Velocity versus depth for the upper Monterey, middle Bengal and Nicobar Deep Sea Fan stations.

TABLE 2. Regression Coefficients of the Predicted Travel Time Curve, with Time as the Independent Variable

(i.e. $X = A_1 T + A_2 T^2 + A_3 T^3 + A_4 T^4$)

	Monterey Fan	Bengal Fan	Nicobar Fan
A_1	1554.8±9.0	1503.5±1.2	1513.7±12.2
A_2	24.875±18.6	130.3±12.3	245.5±61.1
A_3	33.8±12.0	8.2±6.0	-13.1±52.4
A_4	-2.6±2.1	2.8±0.7	7.8±11.3

Data of the Bengal and Nicobar Fan from Dorman and Jacobson (1981) and Jacobson et al. (1984), respectively. Unit of X is meters and T is seconds.

From the velocity gradient profile of the upper Monterey Fan (Fig.15), a small increase of velocity gradient was noted at the deepest part of the Monterey Fan sedimentary structure. This anomalous increase indicates the progradation of deep sea fans which hypothesizes the fan subunits will progress further away from the source as the fan grows. A distal sediment with lower porosity will be buried by the prograding sediments with higher porosity. Therefore, old sediments with distal characteristics should be found under the newly deposited proximal sediments. The whispering gallery phases contribute critical information in determining the sediment velocity structure of the upper Monterey Fan. The basic assumption in identifing these multiples were that these multiple-path refraction waves bottomed in shallow depth with large amplitudes and were caused by the high velocity gradient structure. The resultant velocity model shows that all those whispering gallery phases were traveling within the uppermost layer (485 m of depth) with velocity gradient of 0.875 s^{-1} - 0.650 s^{-1}.

Sheriff and Geldart (1983) reviewed the factors which influence seismic velocity, such as effect of lithology, density, porosity, depth of burial and pressure, age, frequency, temperature and interstitial fluid. Investigating the lateral velocity variations, we can disregard several factors which will be invariant among the fan subunits. Hamilton (1979) examined seismic velocity of marine sediments and stated that the influential factors are the pressure-induced porosity reductions and effects on the sediment mineral from the temperature increases due to heat flow, the rigidity increase caused by lithification, and the pore-water pressure increases. Sheriff and Geldart (1983) concluded that porosity is the most important factor in determining the velocity in a sedimentary rock. Sediment velocities have a dependence upon interstitial fluids due to the very high porosities. On the sea floor, sediments from continental terrace environment have

typical porosities of 38.6% for coarse sand, 54.2% for silty sand, 66.3% for sand-silt-clay, 73.0% for silty clay and 80% for silty clay in abyssal plain. In the shallow depth of deep sea fan, the interstitial fluid, mainly sea water, should strongly dominate the seismic velocity than other factors. Among fan subunits, different porosity structures can be formed due to different sedimentation rates, which is related to the distance from the sediment source. Berner (1980) stated that the rapidly deposited sediments have less time to adjust to the overburden pressure and, as a result, the water content is higher. Furthermore, the water content is often a good qualitative indication of deposition rate for surface muds. A area with higher sedimentation rate should result in sediment structure with high porosity because that continuously depositing sediments, which always contain high water content, will block the deposited sediments and prohibit the expulsion of pore water of sediments to reach an equilibrium porosity condition.

Two common mineral-grain structure of marine sediments are the mixed grain structure for sands, silty sands, and sandy silts with mixtures of sand, silt, and clay in various proportions and the cardhouse structure for silty clay or clayly silt, which normally is a clay matrix with silt or sand particles (Hamilton and Bachman,1982). The gravity cores (Hess and Normark, 1976) on the levee bank of the Monterey fan-valley show an interbedded structure with sand-silt and clay layers. At the distal parts of fans, finer sediments , such as silty clay and clay, are the most common sediment and have slightly higher porosities than the sand-silt-clay. However, the higher porosity in the distal part of fans due to the grain size is opposite to the observed porosity profiles of the three fan subunits, which indicate lower porosities for the lower fan subunits. Obviously, porosity increases with decreasing grain size, and the distribution of grain size of

sediments, which shows mostly fine grain sediments on the lower fan, would not help to explain the observed porosity variations among the three fan subunits. The typical deep sea fan sediments consist of sand layers with interbedded finer grained sediments. Due to the interbedded structure, the porosity profiles determined from refraction profiles are actually averaged out layers of different grain sizes and does not reflect the porosity from a layer with single grain size. The difference in grain size and its effect in porosity are diluted by the interlayered structure. The different sedimentation rates, therefore, seem to be the most possible and reasonable cause to explain why the porosity decreases with increasing distance from the sediment source.

Velocity gradients measured in the Bengal Fan by the sonobuoy technique were reported by Bachman et al. (1983). The near-surface velocity gradient of the Bengal Fan was low in the upper fan (0.86 s^{-1}), high in the central fan (1.94 s^{-1}), and again lower in the southern fan (1.18 s^{-1}), and 1.62 s^{-1} in the Nicobar Fan. Minimum velocity gradients were found in those areas where sedimentation rates were high, since sediments accumulated in thick section have not had time to fully consolidate. This interpretation agrees with the result in this research that the sedimentation rates are the responsibility of the variations of porosity. Comparing the near-surface velocity gradients of Bachman's et al.(1983) with the surface velocity gradient of the three fan subunits reported here, rather closely agreeing velocity gradients are found. The upper Bengal Fan surface velocity gradient (0.86 s^{-1}) compares favorably with the upper Monterey Fan (0.875 s^{-1}). Similarily, the middle Bengal Fan surface velocity gradient of Bachman's et al.(1983) 1.94 s^{-1} compares with 1.87 s^{-1} found by Dorman and Jacobson (1981). However, a significant difference of the velocity gradient in the Nicobar Fan was noted, 1.625 s^{-1} from Bachman et

al.(1983) and 2.32 s^{-1} from Jacobson's et al.(1984). Magara (1976) studied the water expulsion from clastic sediments during compaction and pointed out a fault or vertical high porosity sand body may act as a fluid conduit to transport the fluid upward. The difference can be caused by the presence of a fault within 1 km of the refraction site on the Nicobar Fan, which probably acts as a vertical conduit for fluid transport.

Velocity gradients in a thick sediment layer are usually positive, parabolic and decrease with depth in the sediments (Ewing and Nafe, 1963) The velocity gradient profiles from the three different fan subunits show the same characteristic as described above; furthermore, the distinct asymptotic gradients reveal one or more factors are acting among those fan subunits during the fan growth period yielding the lateral velocity variations. We examined the causes of the lateral variations of sediment seismic velocities, which can relate with the various deep sea fan models. Numerous submarine fan models have been proposed, but only two models are widely quoted and debated in the literature, that is, Mutti and Ricci Lucchi's from ancient fan studies (Mutti and Ricci Lucchi, 1972) and Normark's from modern fan studies (Normark 1970a, 1978). Both models have been discussed in the previous "Deep Sea Fan Models" chapter, and only the factors which influence the seismic velocities of sediments will be discussed.

Mutti and Ricci Lucchi (1974) proposed a modified model, a detached-lobe fan model, where sediments bypass the middle fan area and are deposited on the lower fan. This modification came from the study of the Eocene Hecho group in Spain. Bachman et al. (1983) found that the velocity gradient was lower for the southern Bengal Fan (1.185 s^{-1}) than for the central Bengal Fan (1.945 s^{-1}) ,and a median value, 1.625 s^{-1}, for the fossil lower fan, the Nicoban Fan. The lowest value of the surface velocity

gradient, 0.865 s^{-1} was found for the upper Bengal Fan. They concluded that the minimum velocity gradients were found in the region of the highest rates of sediment accumulation. Therefore, the low gradients measured in the south Bengal Fan favor the Mutti and Ricci-Lucchi's deep sea fan model. So far, the bypass model has caused many debates. When the turbidity current spreads out from a channel, it is very possible that the current will slow down, resulting in deposition rather than bypassing. Walker (1980) pointed out that the channels gradually decrease their topographic expression down fan. It is possible that the turbidity currents are spilling out of the channels before the ends are reached and are depositing sediment as inter-channel thin-bedded turbidite facies. Shanmugam and Moiola (1985) stated that the bypass model is strongly related with the basement topography, as evidenced in the growing Boltana anticline in Mutti and Ricci Lucci's study in Spain. The effect of the tectonic influence, a sudden rise in slope, was examined with an excellent schematic illustration of the hydralic jump case (Shanmugam and Moiola,1985; Fig.3A-D). The bypass fan model (the detached-lobe model) belongs to the highly efficient fan system (Johns and Mutti, 1981), also called the enlongate fan system (Nelson and Kulm, 1973). The Bengal Fan, which has a river-delta as the sediment source with a high mud-sand ratio sediment is the best example of the highly efficient or elongate fan system. However, no obvious bypass zone is present.

The two significant morphologic features, the bypass zone of the Mutti and Ricci Lucchi's fan model and the suprafan of the Normark's fan model, are still controversial. More studies on various deep sea fans are needed. Studies of ancient fan are limited by isolated outcrops, and structural disruption cannot offer a complete description. So further studies will depend upon extensive and detailed long cores on modern deep sea fans

with complete seismic studies to solve these controversies.

The Normark model suggests a suprafan feature where most of the coarse turbidites are deposited. The Mutti and Ricci Lucchi's model hypothesizes a bypassing zone in the middle fan and that deposition is more likely to happen on the lower fan. Unfortunately neither of these models has clearly predicted the pattern of sedimentation rates over the whole of deep sea fans. Nazarkin (1979) reviewed studies on the influence of sedimentation rate on geological processes in modern sedimentary basins and indicated that the degree of diagenetic alterations of sedimentary mineral components and associated organic matter in sedimentary deposits is a direct function of sedimentation rate and its duration. Larsen and Chilingar (1983) pointed out that sedimentation rate controls the degree of compaction of sediments and determines direction, dynamics, and degree of organic matter alternation during diagenesis, which influence the intensity of hydrocarbon generation. Hamilton et al. (1977) interpreted the lower velocity gradients in the north and west Bengal Fans as the area with higher depositional rates, and less consolidation and lithification near the riverine source area of the sediments. Bachman et al. (1983) indicated the minimum velocity gradient of the Bengal Fan was found in those areas where sedimentation rates were the highest, i.e. the upper or the north Bengal Fan.

Berner (1980) pointed out the initial porosity of sediments at the time of sedimentation is primarily a function of grain size. The behavior during compaction of sands and clays is significantly different due to the differences in initial packing. In the upper few hundred meters, sand undergoes only minor particle reorientation but the clay-rich sediments undergo continual compaction with large porosity reductions. The cardhouse structure with silt- and sand-size particles suspended in a clay

matrix (Hamilton and Backman,1982, Fig 4e) is the typical sediment grain structure in the levee or overbank regions. The weight of overlying sediments begins to force mutually repelling particles closer together and to collapse the cardhouse structure. During active periods, the turbidity current gradually lose its light sediment grains, such as clay, silt and fine sand due to the overbank flow. Those overbank sediments, mostly fine grain sediments, carry significant water content when deposited on the sea floor. The cardhouse sediment structure, a high porosity grain structure, will result in low velocity gradients. In areas of high sedimentation rates, the deposited sediments always will be covered by the continuously depositing sediments so the extra pore water cannot be expelled out by the overburden pressure. Therefore, a high porosity sediment structure will result in the high sedimentation-rate area.

The velocity-gradients profiles from each fan subunit (the upper Monterey Fan, the middle Bengal Fan, and the Nicobar Fan as the fossil lower fan) reveal a systematic decreasing sedimentation rate pattern. However, the presence of a normal fault within 1km of the Nicobar Fan station prohibits us from drawing a definite conclusion. The effect of the fault may act as pore water conduit and can lead to extremely low porosities in the fossil lower fan. By examining the controversy of velocity measurements in the Bengal Fan Complex, two factors which influence the seismic response are probably responsible. First, the Bengal Fan has many characteristics which classify it as belonging to the highly efficient fan system, and the bypass hypothesis from Mutti and Ricci Lucchi suggests most sediment may deposit on the lower fan subunits. However, the presence of the 2500 km long channel which cut throughout the entire Bengal fan suggests that no bypassing zone may exist. Second, the Nicobar Fan has not received any turbidite sediments in the past 6 M.Y.,

and since then, only a thin layer (about 6 m) of pelagic sediment with some volcanic ash has been deposited. The surface velocity gradient may be affected by this local tectonic effect; therefore, only the data from the deeper structure can reflect the characteristics of the fan growth period. Another refraction profile further away from the fault is critically important to evaluate both the effects of the presence of a fault, which may act as a pore water conduit, and the relative rates of sediment accumulation, which can determine the validity of the bypass hypothesis in the Nicobar Fan.

Plots of velocity, density, porosity, and simple overburden pressure versus depth are shown in Fig. 23. The density and porosity profiles show a monotonical increase and decrease, respectively, within the first kilometer of depth. There are significant differences among these profiles at equivalent depth; however, the small variation of effective pressure profiles cannot explain the significat variation. From examining these estimated temperature profiles of different fan subunits, the lateral and vertical temperature distributions in a deep sea fan complex are revealed (Fig. 24). The geothermal gradient of the upper Monterey Fan (66 ^{o}C/km) is significantly higher than either the middle Bengal Fan (45^{o}C/km) or the Nicobar Fan (52 ^{o}C/km). The high geothermal gradient can help the genesis of petroleum without deep burial. The temperature at the bottom of the sediment layer on the upper Monterey Fan would be 104 ^{o}C, which is just above the theshold temperature, 97 ^{o}C, of Oligocene sediments. The threshold temperature is the temperature needed for petroleum generation (Connan, 1974). This implies that these buried channels with coarse sand, excellent cover of fine sediments, and a large volume, make a good potential reservoirs for hydrocarbon.

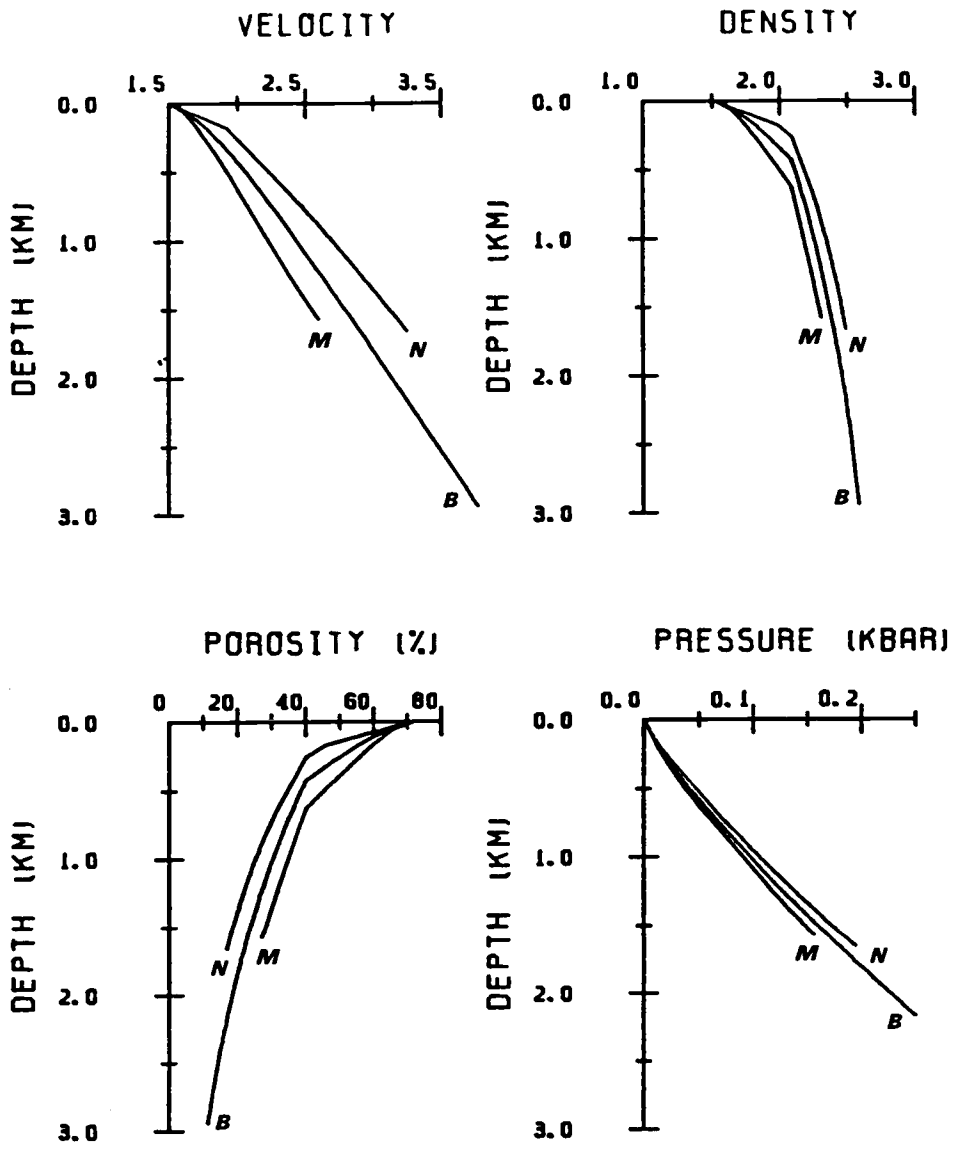

Figure 23. Velocity, density, porosity and simplified overburden pressures for the upper Monterey, middle Bengal and Nicobar Deep Sea Fan stations, as derived from the velocity profiles.

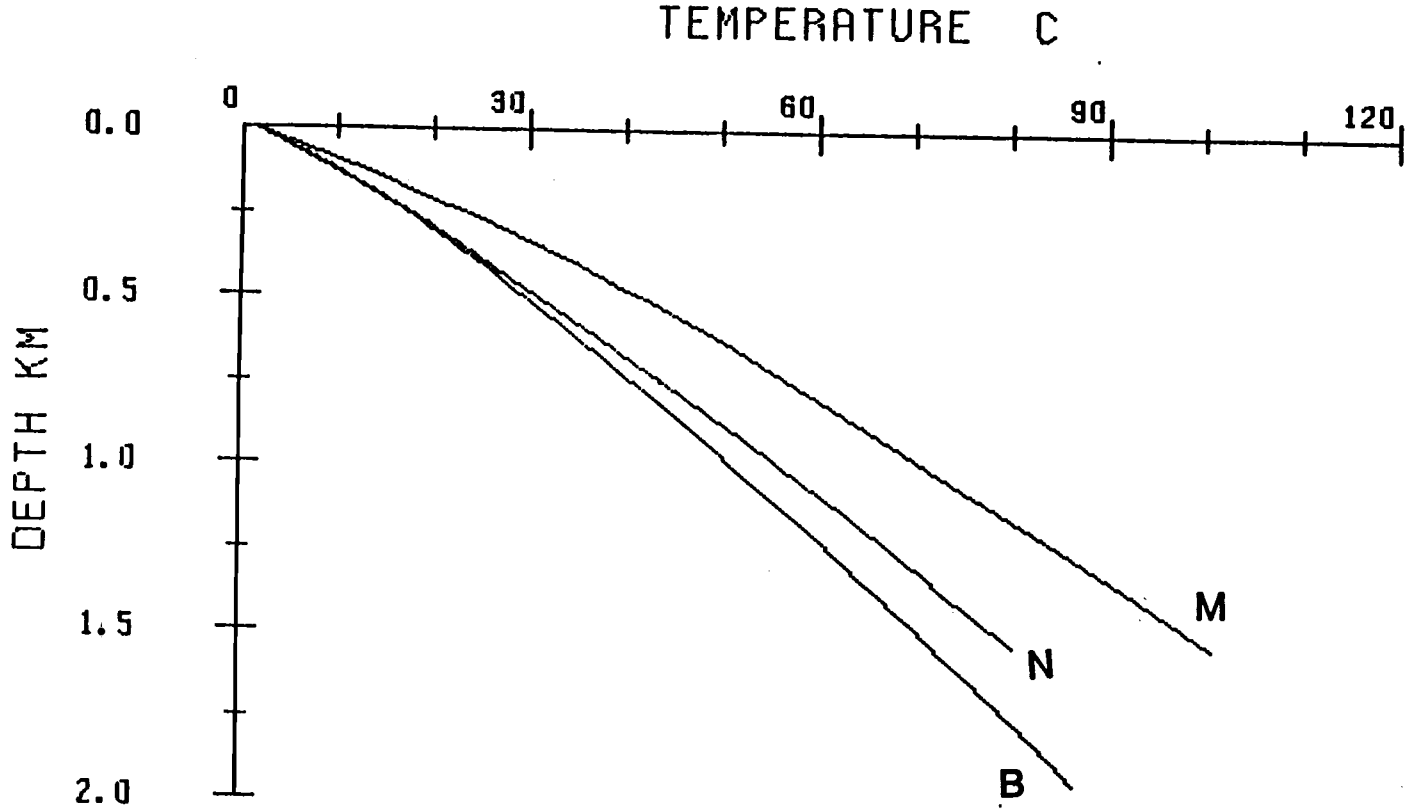

Figure 24. Temperature versus depth functions. M is the Monterey Fan data, B is the Bengal Fan data and N is the Nicobar Fan data.

CONCLUSIONS

A systematic lateral variation is revealed from the velocity gradient profiles from the upper Monterey Fan, the Central Bengal Fan, and the Nicobar Fan as a fossil lower fan. These profiles show remarkable morphologic similarities in trends and significant differences among the asymptotic values. The successful identifications of the whispering gallery phases from the upper Monterey Fan data provide valuable information to evaluate the shallow sediment structures, where most velocity-gradient variations occur. All the velocity gradient profiles show high velocity gradients near sea floor, decreasing rapidly to asymptotic values within 1km of depth. At the bottom part of the sediment structure in the upper Monterey Fan, the velocity gradient actually increases slightly and this may indicate the progradation of the fan growth. From the upper Monterey, the Central Bengal, and the Nicobar Fans, the initial velocity gradients, 0.875 s^{-1}, 1.87 s^{-1}, and 2.32 s^{-1} and the asymptotic velocity gradients at depth. 0.59 s^{-1}, 0.68 s^{-1}, and 0.81 s^{-1} , reveal the seismic characteristics of each fan subunit.

The velocity-depth function of the sediment sequence on the upper part of the Monterey Fan demonstrates a typical deep sea fan velocity function. The velocity structure of the upper Monterey Fan indicates a thick sequence of low velocity sediments overlying a high velocity basement structure. The acoustic basement is probable a pre-fan sediment structure rather than oceanic crust. The 95% confidence bounds were calculated by the linear tau-zeta inverse technique along with the best fitting model. Both the general and "stripping" models show similar results; however, the

general model provids a better estimate of the confidence bounds.

The systematic increases of velocity gradients on deep sea fans suggest that the sedimentation rates are decreasing from proximate to distal areas. Two significant features, the suprafan and the bypassing zone which represent Normark's and Mutti and Ricci Lucch's fan models respectively, were not observed in our geophysical studies. The existence of the bypassing zone, the most significant characteristic of the highly efficient fan system, on the Bengal-Nicobar Fan complex cannot be determined due to the ambiguous effect of the fault nearby the Nicobar Fan station. Similar experiments should be conducted in the Nicobar Fan away from the fault area and also in the southern Bengal Fan . With such a experiment, the two controversial issues can be examined and solved, i.e. can the fault act as a conduit of pore water (Magara,1976) and the importance of bypassing the middle fan (Mutti and Ricci Lucchi, 1974).

Deep sea fans constitute many major hydrocarbon reservoirs around the world, but the studies of the fans to date cannot outline a clear fan model for both modern and ancient deep sea fans. Many morphologic and core studies of modern deep sea fans have been done and presented in the literature; however, the studies of the seismic response of fan sediments are not included. Any future studies of deep sea fans must reconcile the the problems between the results of the ancient and the modern fans, so that a common understanding of deep sea fans can be established.

Shunmugan and Moiola (1985) pointed out that the two widely cited and debated deep sea fan models, Normark's and Mutti and Ricci Lucchi's, can produce similar vertical sequences when the fan progrades. Without confusing with the terminology and surface morphology, the physical properties of vertical structures can distinguish the undistorted characteristics from the original sedimentation. The long cores from Ocean

Drilling Project on deep sea fans can provide the crucial information to examine various problems of deep sea fan studies but cost considerable amounts of money and time. Therefore, the study of lateral velocity variation from refraction profiles, especially the deep structure, can provide the first clues with which to solve the controversies of deep sea fan studies.

BIBLIOGRAPHY

Aki, K., AND P. G. Richards, 1980, Quantitative Seismology Theory and Methods, Vols. I and II, W. H. Freeman and Co., San Franciso, 423.

Atwater, T., 1970, Implications of Plate Tectonics for the Cenozoic Tectonic Evolution of Western North America, Geol. Soc. of Am. Bull., 81, 3513-3536.

Bachman R. T., Hamilton, E. L., and Curray J. R., 1983, Sediment Sound Velocities from Sonobuoys: Sunda Trench and Forearc Basins, Nicobar and Central Bengal Fans, and Andaman Sea Basins: J. Geophys. Res., 88, 9341-9346.

Bee, M., and Jacobson, R. S., 1984, Linear Inversion of Body-Wave Data-Part III: Model Parameterization: Geophysics, 49, 2088-2093.

Berner, R. A., 1980, Early Diagenesis, Princeton University Press, Princeton, N. J., 241.

Bessonova, E. N., V. M. Fishman, V. Z. Ryabuyi, and G. A. Sitnikova, 1974, The Tau Method for Inversion of Travel Times, 1, Deep Seismic Sounding Data, Geophys. J. Roy. Astr. Soc., 36, 377-398.

Bessonova E. N., V. M. Fishman, M. G. Shnirman, G. A. Sitnikova, and L. R. Johnson, 1977, The Tau Method for Inversion of Travel Times, 2, Earthquake Data, Geophys. J. Roy. Astr. Soc. 46, 87-108.

Blatt, H., Middleton, G. V., and Murray, R. O., 1972, Origin of Sedimentary Rocks,, Prentice-Hall, Inc., Englewood Cliffs, N. J., 634.

Bouma, A. H., 1962, Sedimentology of Some Flysch Deposits: A Graphic Approach to Facies Interpretation. Amsterdam, Elservier., Netherlands, 168.

Bullard, E. C., 1963, The Flow of Heat Through the Floor of the Ocean, in The Sea, V. 3: The Earth Beneath the Sea, ed. M. N. Hill, Wiley, New York, 218-232.

Cernock, P. T., 1970, Sound Velocities in Gulf of Mexico Sediments as Related to Physical Properties and Simulated Overburden Pressure, Dept. of Oceanography Tech. Rept., 70-5-T. Texas A&M Univ.

Cerveny, V. and R. Ravindra, 1971, Theory of Seismic Head Waves, University Toronto Press., Toronto, 205.

Chase, T. E., Normark, W. R., and Wilde, P., 1975, Oceanographic Data of the Monterey Deep Sea Fan, University California Inst. Marine Resources Tech. Report. TR-58, 2.

Choy, G. L., 1977, Theoretical Seismograms of Core Phases Calculated by a Frequency-Dependent Full Wave Theory, and Their Interpretation: Geophys. J. Roy Astr. Soc., 51, 275-311.

COMFAN, 1984, Geo-Marine Lett., 3, No 2-4.

Connan, J., 1974, Time-Temperature Relation in Oil gensis; A.A.P.G. Bull., 58, 2516-2521.

Cormier, V., and Richards, P. G., 1977, Full Wave Theory Applied to a Discontinuous Velocity Increase; The Inner Core Boundary: J. Geophys. Res., 43, 3-31.

Curray, J. R., F. J. Emmel, D. G. Moore, and W. Raitt, 1982, Structure, Tectonics, and Geological History of the Northeastern Indian Ocean: The Ocean Basins and Margins, V. 6, The Indian Ocean, A. M. Nairn and F. G. Stehli ed., Plenem Press, N. Y., 399-450.

Dill, P. F., Dietz, R. S., and Stewart, H., 1954, Deep-Sea Channels and Delta of the Monterey Submarine Canyon: Bull. Geol. Soc. Am., 65, 191-194.

Dorman, L. M., 1979, A Linear Relationship between Earth Models and Seismic Body Wave Data: Geophys. Res. Lett., 6, 132-134.

Dorman, L. M., 1983, Modelling and Parameterization Error in Body Wave Seismology: Geophys. J. Roy. Astr. Soc., 72, 571-576.

Dorman, L. M., and Jacobson, R. S., 1981, Linear Inversion of Body Wave Data-Part I: Velocity Structure from Traveltimes and Ranges: Geophysics, 46, 138-151.

Emmel, F. J. and J. R. Curray, 1981, Channel Piracy on the Lower Bengal Fan: Geo-Marine Lett., 1, 123-127.

Ewing, M., Ericson, D. B., and Heezen, B. C., 1958, "Sediments and Topography of the Gulf of Mexico" in Habitat of Oil. A Symposium. ed. L. G. Weeks, A.A.P.G. Bull., 957-1053.

Ewing, J. I. and J. E. Nafe, 1963, The Unconsolidated Sediments: in the Sea, Vol. 3: The Earth Beneath the Sea, edited by M. N. Hill, Wiley, New York, 73-84.

Goodman, D., 1983, Seismic Refraction Survey of Crustal and Upper Mantle Structures in the West Philippine Basin, M.S. thesis, College of Oceanography, Oregon State University, 122.

Hamilton, E. L., 1970, Prediction of in Situ Acoustic and Elastic Properties of Marine Sediments, North Pacific, J. Geophys Res., 75, 4423-4446.

Hamilton, E. L., 1976, Variations of Density and Porosity with Depth in Deep-Sea Sediments: J. Sed. Petrology, 46, 280-300.

Hamilton, E. L., 1978, Sound Velocity-Density Relations in Sea-Floor Sediments and Rocks: J. Acoust. Soc. Am., 63, 366-377.

Hamilton, E. L., 1979, Sound Velocity Gradients in Marine Sediments, J. Acoust. Soc. Am., 65, 909-922.

Hamilton, E. L., and Bachman, R. T., 1982, Sound Velocity and Related Properties of Marine Sediments, J. Acoust. Soc. Am., 72, 1891-1904.

Hamilton, E. L., Moore, D. G., Buffington, E. C., and Sherrer, P. L., 1974, Sediment Velocities from Sonobuoys: Bay of Bengal, Bering Sea, Japan Sea, and North Pacific: J. Geophys. Res., 79, 2653-2668.

Hamilton, E. L., R. T. Buchman, J. R. Curray, and D. G. Moore, 1977, Sediment Velocities From Sonobuoys: Bengal Fan, Sunda Trench, Andaman Basin,and Nicobar Fan: J. Geophys. Res., 82, 3003-3012.

Hess, G. R., 1974, Submarine Fanfare: A Comparison of Modern and Miocene Deep Sea Fans, M.S. thesis, Univ. Minnesota, 118.

Hess, G. R., and Normark, W. R., 1976, Holocene Sedimentation History of the Major Fan Valleys of Monterey Fan: Marine Geology, 22, 233-253.

Hill, D. P., 1971a, Velocity Gradients and Anelasticity from Crustal Body Wave Amplitudes: J. Geophys. Res. 76, 3309-3325.

Hill, D. P., 1971b, Velocity Gradients in the Earth's Crust from Head-Wave Amplitudes. J. Geophys. Res. 76, 3309-3325.

Houtz, R. E., 1974, Preliminary Study of Global Sediment Sound Velocities from Sonobuoy Data, in the Physics of Sound in Marine Sediments, ed. L. Hampton, Plenum, N. Y., 519-535.

Houtz, R. E., 1977, Sound-Velocity Characteristics of Sediment from the Eastern South American Margin: Geol. Soc. Am. Bull., 88, 720-722.

Houtz, R. E., 1978, Preliminary Sonobuoy Study of Rapidly Accumulating Shelf Sediments: J. Geophys. Res., 83, 5397-5404.

Houtz, R. E., 1980, Results and Methods Used to Determine the Acoustic Properties of the Southeast Asia Margins, in Bottom-Interacting Ocean Acoustics, ed. W. A. Kuperman and F. B. Tenseen, Plenum, N. Y., 99-109.

Houtz, R. E., 1981, Comparison of Sediment Sound-Velocity Functions from Conjugate Margins, Geol. Soc. Am. Bull., 92, 262-267.

Jacobson, R. S., Shor. G. G. Jr., and Dorman, L. M., 1981, Linear Inversion of Body Wave Data-Part II: Attenuation Versus Depth using Spectral Ratios: Geophysics, 46, 152-162.

Jacobson, R. S., Shor, G. G., Jr., and Bee, M., 1984, A Comparison of Velocity and Attenuation between the Nicobar and Bengal Deep Sea Fans: J. Geophys. Res., 89, 6181-6196.

Johns, D. R. and Mutti E., 1981, Facies and Geometry of Turbidite Sandstone Bodies and Their Relationship to Deep Sea Fan Systems. Abstracts, International association of Sedimentologists 2nd European Regional Meeting, Bologna, Italy, p. 89.

Johnson and Gilbert, 1972, Inversion and Inference for Teleseismic Ray Data, Methods Comput. Phys., 12, 231-266.

Larsen, G. and G. V. Chilingar, 1983, Diagenesis in Sediments and Sedimentary Rocks, 2, Elsevier, 572 .

Laughton, A. S., 1954, Laboratory Measurements of Seismic Velocities in Ocean Sediments, Proc. R. Soc. London Ser., 336-341.

Laughton, A. S., 1957, Sound Propagation in Compacted Ocean Sediments, Geophysics, 22, 233-260.

Magara, K., 1976, Water Explusion from Clastic Sediments during Compaction-Directions and Volumes: A.A.P.G. Bull., 60, 543-553.

Menard, H. W., 1955, Deep-Sea Channels, Topography, and Sedimentation: A.A.P.G. Bull., 39, 236-255.

Menard, H. W., 1960, Possible Pre-Pleistocene Deep-Sea Fans off Central California, Bull. Geol. Soc. Am., 71, 1271-1278.

Menke, W. H., 1984, Geophysical Data Analysis, Academic Press, Inc., Florida., 260.

Menke, W. H., and Richards, P. G., 1980, Crust-Mantle Whispering Gallery Phases: A Deterministic Model of Teleseismic Pn Wave Propagation: J. Geophys. Res., 85, 5416-5422.

Mutti, E., 1979, Turbidite et Cones Sous-Marine Profounds, in: P. Homewood (ed.) Sedimentation Detrique (Fluviatile, Littorale et Marine). Institute of Geology, Unversity de Fribourg, 353-419.

Mutti, E., and Ricci-Lucchi F., 1972, Turbidites of the Northern Apennines; Introduction to Facies Analysis: Internat. Geology Rev., 20, 125-160.

Mutti, E. and F. Ricci Lucchi, 1975, Turbidite Facies and Facies Associations in: Examples of Turbidite Facies and Facies Associations from Selected Fromations of the Northern Apennines Field Trip Guidebook A-11. International Sedimentological Congress IX. Nice, 31-36.

Naval Ordnace Systems Command, Rep. NAVORD OP 3696, Technical Manual; Explosives Safety Precautions for Research Vessels, Washington D.C., 1973.

Nazarkin, L. A., 1979, Influence of Sedimentation Rate and Erosional Section on Oil and Gas Potentials of Sedimentary Basin. Saratoo University, 336.

Nelson, C. H., and Kulm, L. D., 1973, Part II: Submarine Fans and Deep-Sea Channels, in Turbidites and Deep-Water Sedimentation: SEPM Pacific Sec., Short Course Notes, Anaheim, California, 39-70.

Normark, W. R., 1970a, Growth Patterns of Deep Sea Fans: A.A.P.G. Bull., 54, 1094-1101.

Normark, W. R., 1970b, Channel Piracy on Monterey Deep-Sea Fans: Deep-Sea Research, 17, 837-846.

Normark, W. R., 1978, Fan Valleys, Channels, and Depositional Lobes on Modern Submarine Fans: Characters of Recognition of Sandy Turbidite Environments: A.A.P.G. Bull., 62, 912-931.

Normark, W. R., Hess, G. R., Stow, D. A. V., and Bowen, A. J., 1980, Sediment Waves on the Monterey Fan Levee: A Preliminary Physical Interpretation: Marine Geology, 37, 1-18.

Normark, W. R., Cutmacher, C. E., Chase, T. E., and Wilde, P., 1984, Monterey Fan: Growth Pattern Control by Basin Morphology and Changing Sea Levels: Geo-Marine Lett., 3, 93-99.

Ostle B. and R. W. Mensing, 1975, Statistics in Research. The Iowa State University Press, Iowa, 596.

Parsons, B. and J. G. Sclater, 1977, An Analysis of the Variations of Ocean Bathymetry and Heat Flow with Age: J. Geophy. Res., 82, 803-827.

Rayleigh, T. W. S., 1910, The Problem of the Whispering Gallery, Philosophical Magazine, 20, 1001-1004.

Sclater J. G. and R. L. Fisher, 1974, Evolution of the East Central Indian Ocean, with Emphasis on the Tectonic Setting of the Ninetyeast Ridge: Geol. Soc. of Am. Bull., 85, 683-702.

Shanmugam, G., and R. J. Moiola, 1985, Submarine Fans and Related Turbidite Systems; edited by A. H. Bouma, W. R. Normark, and N. E. Barner, Springer-Verlag, New York., 355.

Shepard, F. P., 1966, Meander in Valley Crossing a Deep Sea Fan: Science, 154, 385-386.

Shepard, F. P., and Dill, R. F., 1966, Submarine Canyons and Other Sea Valleys, Rand McNally, Chicago., 381.

Sheriff,R. E. and L. P. Geldart, 1983, Exploration Seismology, Vol. 2, Cambridge University Press, Cambridge., 310.

Shor, G. G. Jr., Menard, H. W., and Raitt, R. W., 1971, Structure of the Pacific basin, in the Sea V. 4, Part II, A. E. Maxwell ed., Wiley, New York, 3-27.

Spudich, P., and Orcutt, J. A., 1980, A new Look at the Seismic Velocity Structure of the Oceanic Crust, Rev. Geophys. Space Phys., 18, 627-646.

Stephen, R. A. and A. J. Harding, 1983, Travel-Time Analysis of Borehole Seimic Data. J. Geophy. Res., 88, 8289-8298.

Stow D. A. V., D. G. Howell, and C. H. Nelson, 1984, Sedimentary, Tectonic, and Slop-Apron Turbidite Systems, Geo-Marine Lett., 3, No 2-4, 57-64.

Teleford, W. M., L. P. Girdart, R. E. Sheriff, and D. A. Key, 1976, Applied Geophysics, Cambridge Press, Cambridge, U. K, 960.

Walker, R. G., 1978, Deep-Water Sandstone Facies and Ancient Submarine Fans: Models for Exploration for Stratigraphic Traps: A.A.P.G. Bull., 62, 932-966.

Walker, R. G., 1980, Modern and Acient Submarine Fans: Reply, A.A.P.G. Bull., 64, 1101-1108.

Wiggins, R. A., 1972, The General Linear Inversion Problem: Implication of Surface Waves and Free Oscillations of Earth Structure: Rev., Geophy. Space Phys., 10, 251-285.

Wilde, P., 1965, Recent Sediments of the Monterey Deep Sea Fan, Ph.D. Thesis, Harvard Univ., 153P.

Wilde, P., Normark, W. R., and Chase, T. E., 1978, Channel Sands and Petroleum Potential of Monterey Deep-Sea Fan, California: A.A.P.G. Bull., 62,967-983.

Wilson, W. D., 1960, Equation for the Speed of Sound in Sea Water, J. Acoust. Soc. Am., 32, 1357.

APPENDIX

APPENDIX I

THE TAU-ZETA INVERSION TECHNIQUE

The seismic refraction technique consists of measuring travel times and ranges of the waves that have been refracted from the subbottom at several source-receiver distances. In this marine seismic refraction experiment, observations were made of pressure variations due to the seismic waves, generated by an impulsive source. Data processing can be done either by forward modeling or by inverse techniques. A forward modeling is accomplished by adjusting an initial guess of model parameters, which should be tightly constrained by the available geological and geophysical data, to obtain a model with characteristics similar to the observed data. A more formal approach is the inverse technique. This technique can infer the model, such as the velocities of subbottom structure through which rays traveled, from the observated travel time data. To treat the data with inverse techniques usually requires an assumption of lateral homogeneity. From the reflection profile (Fig. 6), a well stratified homogeneous sediment structure exists at the site in the upper part of the Monterey Fan. Therefore, the lateral homogeneity assumption is probably valid.

Many inverse techniques have been proposed and used for years. The tau-zeta travel time inversion technique of Dorman and Jacobson (1981) for seismic refraction data has been successfully developed and applied to obtain the velocity-depth functions for sediments (Dorman and Jacobson,1981; Jacobson et al.,1984) and oceanic crust (Stephen and Harding, 1983). The tau-zeta inversion technique first reparameterizes the

travel time ,T, and range ,X, into the tau τ and zeta ζ form, as:

$$\tau(p) = T - pX \qquad \zeta(p) = T + pX \qquad \text{(A1)}$$

where p is the horizontal slowness with which the seismic wave travels. Using the tau-zeta combinations of the raw data, T and X, Dorman and Jacobson (1981) showed that errors of tau and zeta are orthogonal, or that the errors in tau are independent of the errors in zeta. This reparamenterization eliminates the multiplicity from the triplication of X(T) or T(X) when a major change of the velocity gradient occurs at depth. The horizontal slowness, which can be derived from the slope of travel time curve, is used as the independent variable. The errors in determinating slowness from the travel time curve do not cause significant errors in $\tau(p)$ but in $\zeta(p)$ (Dorman and Jacobson, 1981). The delay time function, $\tau(p)$, which is simply related to the depth, has played an important role in determining the velocity-depth function for many years (Johnson and Gilbert, 1972; Bessonova et al., 1974, 1976) . By inverting $\tau(p)$ and $\zeta(p)$ together, a tighter bound on the velocity depth function are obtained than by only inverting $\tau(p)$.

Some other advantages of using the tau-zeta linear inversion are the propagation in the errors of the data space into the errors of the solution space and the ability to trade off resolution with the error estimates in the model. The existence of the linear relationship between the model parameters and the data, allow us to use the linear inverse technique. The linear relationship of tau and zeta to a stack of laterally homogeneous layers each with a constant velocity gradient $(dV/dz)_j$ has been

domonstrated (Dorman and Jacobson, 1981). For a multiple layered model, the tau and zeta may be derived as follows:

The derivation of the tau-zeta linear inversion starts with the integral equations relating observables to unknown solutions

$$X(p) = 2p \int_0^{z(p)} V \, (1-p^2V^2)^{-1/2} \, dZ \qquad \text{(A2a)}$$

$$T(p) = 2p \int_0^{z(p)} V^{-1} \, (1-p^2V^2)^{-1/2} \, dZ \qquad \text{(A2b)}$$

This is the standard two-way travel equations for range and travel time when sources and receivers are at the same datum level (Teleford et al., 1976, Eq. 4.43). The aim is to produce a matrix equation relating the model paramaters to the observations, travel times and ranges. Replacing the integration variable dZ in the above equations, Eq.(A2a and b), by (dZ/dV)dV results in

$$X(p) = \int_{V_0}^{V=1/p} 2 \, V \, (1-p^2V^2)^{-1/2} \, dZ/dV \, dV \qquad \text{(A3a)}$$

$$T(p) = \int_{V_0}^{V=1/p} 2p \, V^{-1} \, (1-p^2V^2)^{-1/2} \, dZ/dV \, dV \qquad \text{(A3b)}$$

The function dZ/dV can now be expanded in terms of a set of basic functions $f_j(V)$ (Dorman, 1979)

$$dZ/dV = \sum_j \omega_j \, f_j(V) \qquad f_j(V) = \begin{cases} 1 & v_{j-1} \le v < v_j \\ 0 & \text{elsewhere} \end{cases} \qquad \text{(A4)}$$

where $\omega_j = (dZ/dV)_j$. The choice of each V_j is essentially arbitrary except that V_0 must be the surface velocity. The choice of the velocity at the layer boundaries is important to obtain the best solution; this problems was examined by Bee and Jacobson (1984) and will be reviewed later.

Substituting (A4) into (A3a) and (A3b) gives

$$X(p) = \sum_j \omega_j \left[2 \int_{V_{j-1}}^{V_{lim}} V \, (1-p^2V^2)^{-1/2} \, dV \right] \qquad \text{(A5a)}$$

$$V_{lim} = \text{Min}(V_j, 1/p)$$

$$T(p) = \sum_j \omega_j \left[2 \int_{V_{j-1}}^{V_{lim}} V^{-1} \, (1-p^2V^2)^{-1/2} \, dV \right] \qquad \text{(5Ab)}$$

where ω_j is $(dZ/dV)_j$ and V_{lim} is the smaller value of V_j and $1/p$. Thus there are two equations based on the constant velocity gradient layer structure.

The zeta form is:

$$\zeta(p) = T + pX \qquad \text{(A6a)}$$

$$= \sum_j (dZ/dV)_j \, 2 \left[\int_{V_{j-1}}^{V_{lim}} \frac{dV}{V\,(1-p^2V^2)^{1/2}} + \int_{V_{j-1}}^{V_{lim}} \frac{p\,V\,dV}{(1-p^2V^2)^{1/2}} \right]$$

Evaluating the two integrals in the above equation, Eq(A6a)

$$\zeta(p) = \sum_j (dZ/dV)_j \; 2 \left[\ln \frac{1+(1-p^2V^2)^{1/2}}{V} + (1-p^2V^2)^{1/2} \right] \Bigg|_{V_{lim}}^{V_{j-1}} \qquad \text{(A6b)}$$

$$= \sum_j (dZ/dV)_j \, 2 \left[\ln \frac{V_{lim}\,(1+(1-p^2V_{j-1}{}^2)^{1/2})}{V_{j-1}\,(1+(1-p^2V_{lim}{}^2)^{1/2})} + (1-p^2V_{j-1}{}^2)^{1/2} - (1-p^2V_{lim}{}^2)^{1/2} \right]$$

Similarly, tau can be written as

$$\tau(p) = T - pX$$

$$= \sum_j (dZ/dV)_j \, 2 \left[\int_{V_{j-1}}^{V_{lim}} \frac{dV}{V\,(1-p^2V^2)^{1/2}} - \int_{V_{j-1}}^{V_{lim}} \frac{pV\,dV}{(p^2-V^2)^{1/2}} \right] \qquad \text{(A6c)}$$

where the summation is over j layers. The linearity of zeta and tau with inverse velocity gradients $(dZ/dV)_j$ for each layer, is readily observed. Bee and Jacobson (1984) discussed a "constrained model" in which the velocities at the layer boundaries are the velocities of the observed

refracted waves. These velocities bounding the layers gave the best velocity gradient solution compared to an original assumed model. Each wave spends most of its travel time near its bottoming depth, so most of its information is from that depth range. The "constrained model" was chosen, because it provides a better solution than unconstrained case as dissussed by Bee and Jacobson (1984).

Using the notation of Wiggins (1972), whose linear inversion technique will be followed, $\tau_i(p)$ and $\zeta_i(p)$ are the data c_i, the inverse velocity gradient $(dz/dv)_j$ is the solution x_j, and the bracketed terms of equation (A6a) and (A6b) are the partial derivatives of the observable c_i with respect to the parameter x_j, $(\partial c_i/\partial x_j)$. The linear equations may be written as a matrix

$$A\ X = C \qquad \text{(A7)}$$

where $A_{ij}=\partial c_i/\partial x_j$. Wiggin's linear inverse theory can be fully exploited using a parameter weighting matrix W for the solution X and a covariance matrix S for the data C. The equation (9) may then be written as a weighted matrix equation:

$$S^{-1/2}\ A\ W^{-1/2}\ W^{-1/2}\ X = S^{-1/2}\ C \qquad \text{(A8)}$$

The parameter weighting matrix W is a diagonal matrix. W_{ii} is inversely proportional to the velocity change in the layer i because variations of parameterrs are proportional to this change. Therefore, $W_{ii}=1/(V_i-V_{i-1})$ and $W_{ij}=0$ if $i\neq j$. The data covariance matrix S is composed by the errors in

zeta and the errors in tau. The errors in tau are simply the differences between the observed tau and the predicted tau (Jacobson et al., 1984, Fig. 8). The errors in tau due to the uncertainty of determining the slowness p are negligible (Dorman and Jacobson, 1981). The error in zeta was first assumed to have a diagonalized form and was improved by evaluating the data covariance matrix by the "direct approach" (Jacobson et al., 1984).

$$\sigma\zeta = 2 \left[\frac{\partial^2 X}{\partial T^2}\right]^{-1} \sigma V \qquad \text{(A9)}$$

The data covariance matrix S can be decomposed to calculate $S^{-1/2}$. A minor problem occured when some eigenvalues of S were negative, due to Cov(ζ) being rank deficient. This problem was solved by damping the eigenvalues. This was achieved by using a method described by Jacobson et al. (1984), adding a small positive value to make all the eigenvalues positive. This method, damped least squares, result in a very similar resolution matrix to that found by using the value decomposition method with a cut-off region of nonzero singular values (Menke, 1985, written communication).

The weighted matrix equation was sloved to find the solution vector X. The new A' matrix, $S^{-1/2}\, A\, W^{1/2}$, decomposed by the eigenvector decomposition into

$$A' = U \Lambda V^T \qquad \text{(A10)}$$

where the matrices U and V are used to define orthogonal eigenvectors in

the data and model spaces respectively, and Λ is the diagonalized matrix of eigenvalues. The solution vector X, the inverse velocity gradients, will be

$$X = W^{1/2}\ V\ \Lambda^{-1}\ U^T\ C' \qquad \text{(A11)}$$

where $C' = S^{1/2}\ C$. The natural generalized inverse G^{-g} (Menke, 1984) may be written as

$$G^{-g} = W^{1/2}\ V\ \Lambda^{-1}\ U^T\ S^{-1/2} \qquad \text{(A12)}$$

so that

$$X = V'\ \Lambda^{-1} U'^T\ C = G^{-g}\ C \qquad \text{(A13)}$$

where $V'=W^{1/2}\ V$ and $U'= S^{1/2}\ U$. The covariance matrix of X is

$$\text{Cov}(X) = G^{-g}\ [\text{Cov}(C)]\ G^{-gT} = S\ V'\ \Lambda^{-2}\ V'^T$$

$$= W^{1/2}\ V\ \Lambda^{-2}\ V^T\ W^{1/2} \qquad \text{(A14)}$$

The data resolution matrix, N, indicates whether the data can be independently predicted, or resolved; $d^{pre} = N\ d^{obs}$ where d is the data. N can be written as

$$N = G\ G^{-g} = \{ U'\ \Lambda\ V'^T \} \{ V'\ \Lambda^{-1}\ U'^T \} = U'\ U'^T$$

$$= S^{-1/2} U U S^{-1/2} = U S^{-1} U \qquad \text{(A15)}$$

The model resolution matrix R shows that the estimates of the model parameters are really weighted averages of the true model parameters. As our model parameters are the inverse velocity gradients in order, each row of the resolution matrix can be useful in determining the scale to which features in the model can actually be resolved; $m^{est} = R\, m^{true}$. R can be written as

$$R = G^{-g} G = \{V' \Lambda^{-1} U'^{T}\} \{U'^{T} \Lambda V^{T}\} = V' V'^{T}$$
$$= W^{1/2} V V W^{1/2} = V W V \qquad \text{(A16)}$$

By summing the diagonal element of the data resolution matrix N, n=diag(N) "the important n of data" (Menke, 1984), the percentage of the contribution of zeta and tau to the solution is found. If all eigenvalues are retained, N and R will be diagonal matrices. Chi-square , $\kappa^2 = C' - A' X'$, where $X' = W^{1/2} X$, should close to m-p-1, where m is the number of data and p represents the number of paramenters (Ostle and Mensing, 1975).

The final solution, the velocity depth function, is obtained by integrating the inverse velocity gradient with velocity, like

$$Z(v) = \int_0^{1/p} \sum_j \left[\frac{dZ}{dV}\right]_j dV = \sum_j \left[\frac{dZ}{dV}\right]_j [V_j - V_{j-1}] \qquad \text{(A17)}$$

and

$$\text{Cov}\,[Z(V)] = \alpha\, \text{cov}(x)\, \alpha^{T} + x\, \text{cov}(\alpha)\, x^{T} + 2\, \alpha\, \text{cov}(\alpha, x)\, x^{T} \qquad \text{(A18)}$$

where $\alpha_j = dv_j = (v_j - v_{j-1})$ and $x_j = [dZ/dV]_j$. The $cov(\alpha)$ can be derived from cov(a), the covariance matrix of the coefficients of the travel time curve. $Cov(\alpha,x)$ will be assumed to be equal to zero.